UNIVERSITY OF MINNESOTA
Driven to Discover®

Chronic Wasting Disease- *where it is*

What is Chronic Wasting Disease?

Chronic Wasting Disease (CWD) is a contagious, fatal brain disease affecting wild and farmed cervids such as deer, moose, elk, caribou, and reindeer. The disease is caused by prions, protein material within a deer, that, when folded incorrectly, becomes infectious.
Prions survive for long periods of time in the environment, and they are spread through an infected animal's saliva, blood, feces, urine, and antler velvet. The remains of an animal that dies with CWD can also become a source for new infections.

Where is CWD found?

As of October 2022, CWD in wild and farmed cervids has been reported in 30 states in the United States, as well as in Canada, Norway, Finland, Sweden, and South Korea. For an up-to-date record of where CWD has been found in North America, visit the USGS National Wildlife Health Center website at www.usgs.gov.

CWD is spreading throughout the upper Midwest including North Dakota, South Dakota, Nebraska, Iowa, Illinois, Wisconsin, Michigan and Minnesota. CWD was first identified in Minnesota in farmed elk in 2002 and wild white-tailed deer in 2010. CWD continues to be identified in cervids across Minnesota, becoming endemic in the wild white-tailed deer population in southeastern counties.

What is being done to stop the spread of CWD?

Experts from the University of Minnesota are currently working on developing faster and more available diagnostic tests, researching the way CWD spreads, and analyzing the ecological impacts of the disease.

The Minnesota Department of Natural Resources and the Minnesota Board of Animal Health are surveying and managing CWD in Minnesota and working to limit its spread in wild and farmed cervids across the state.

What should I do if I see a sick deer in MN?

Please report any sick deer by calling 888-646-6367.

Additional Contacts - MNPRO

Email: mnpro@umn.edu
Dr. Peter Larsen, co-director: 806-535-8926 Dr.
Tiffany Wolf, co-director: 612-625-0492
Marc Schwabenlander, associate director: 651-216-1240

See the CWD Transmission and Progression animated video:
https://youtu.be/1utScxaceNg

Location of CWD detections in Minnesota.

Map data current as of December 26, 2022

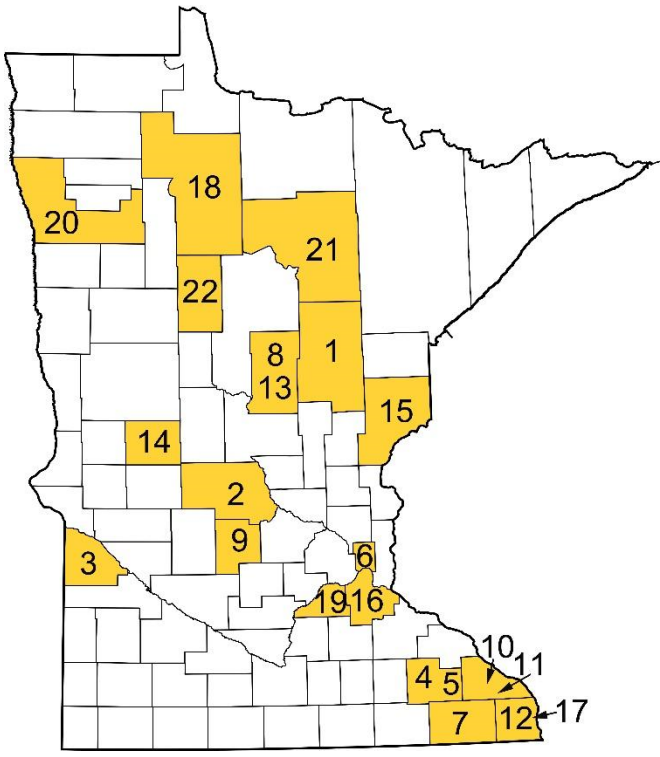

1. 2002 - Aitkin County elk farm
2. 2003 - Stearns County elk farm
3. 2006 - Lac Qui Parle County mixed deer/elk farm
4. 2009 - Olmsted County elk farm
5. 2010, 2019-20 - Olmsted County wild white-tailed deer
6. 2012 - Ramsey County European red deer farm
7. 2016-22 - Fillmore County wild white-tailed deer
8. 2016, 2018 - Crow Wing County deer farm
9. 2017 - Meeker County deer farm
10. 2017 - Winona County deer farm
11. 2018-22 - Winona County wild white-tailed deer
12. 2018-21 - Houston County wild white-tailed deer
13. 2019, 2021 - Crow Wing County wild whitetail deer
14. 2019 - Douglas County deer farm
15. 2020 - Pine County deer farm
16. 2020-21 - Dakota County wild white-tailed deer
17. 2020 - Houston County deer farm
18. 2021 - Beltrami County deer farm
19. 2021 - Scott County wild white-tailed deer
20. 2021- Polk County wild white-tailed deer
21. 2022 - Itasca County wild white-tailed deer
22. 2022 – Hubbard County wild white-tailed deer

UNIVERSITY OF MINNESOTA
Driven to Discover®

Chronic Wasting Disease- *what you can do*

For all - *get informed*

What is Chronic Wasting Disease?

Chronic Wasting Disease (CWD) is a contagious, fatal brain disease affecting wild and farmed cervids such as deer, moose, elk, caribou, and reindeer. The disease is caused by prions, protein material within a deer, that, when folded incorrectly, becomes infectious.
Prions can survive for long periods of time in the environment, and they are spread through an infected animal's saliva, blood, feces, urine, and antler velvet. The remains of an animal that dies with CWD can also become a source for new infections.

What's happening in Minnesota?

Stay up-to-date on CWD in Minnesota through the Minnesota Department of Natural Resources (DNR), the Minnesota Board of Animal Health (BAH), and the Minnesota Center for Prion Research and Outreach (MNPRO).

- DNR - https://www.dnr.state.mn.us/cwd/index.html
- BAH - https://www.bah.state.mn.us/news_release/
- MNPRO - https://mnpro.umn.edu/

For venison consumers - *know the risks*

Can CWD be transmitted to humans?

Currently, there is no direct evidence that CWD poses a risk for humans; however, public health officials at the Center for Disease Control (CDC) recommend that we do not consume meat from animals known to be infected. Because we do not yet know the full risk that CWD poses to humans, it is important that we avoid eating CWD contaminated meat. Determine if the venison you consume was harvested in a CWD management area. If so, wait for CWD "not detected" test results before consuming the meat or avoid consuming the meat if the deer was not tested. The prions that cause CWD are very resistant to heat and freezing temperatures. Cooking or freezing the meat will not remove prions from any infected meat.

For landowners - *be good stewards*

What if CWD is found on my property?

Cooperate with Minnesota DNR and/or BAH officials to better understand the extent of disease on the landscape. The 3D shape of CWD prions makes them almost indestructible. This durability facilitates the spread of prions in the surrounding environment through many avenues, including water, soil, and plants. MNPRO is initiating cutting-edge research on the spread of CWD in the complex ecosystems across Minnesota.

For hunters - *reduce the spread*

What are the CWD regulations?

Minnesota DNR's CWD regulations are an important part of reducing the risk of disease spread across Minnesota and into other states. The CWD regulations fluctuate from year to year as information is obtained about the state of the disease. Carefully read the regulations prior to every hunting season. Current regulations for testing, carcass movement, and feeding bans can be found at licensing centers and the DNR's CWD webpage:
https://www.dnr.state.mn.us/cwd/index.html

What precautions should be taken?

Identification

Most CWD-positive wild deer appear normal. It may take over a year before an infected deer develops symptoms, which can include drastic weight loss (wasting), stumbling, inactivity, and loss of fear of humans. Specifically, deer become thin, drink and urinate excessively, have poor balance & coordination, lack body fat, have drooping ears, and difficulty swallowing. Inability to swallow leads
to pneumonia and death. Please report any sick deer by calling 888-646-6367.

Processing

Consider having your deer processed and wrapped individually, either privately or commercially, so as not to mix CWD-positive and CWD-"not detected" deer meat. When processing your deer, it is important to identify and remove lymph nodes. Lymph nodes accumulate pathogens including prions, the disease causing agent of CWD. A video from Dr. Grant Woods highlights this in segments beginning at 3:41 and 7:18. https://youtu.be/H2UsVd9d8vI

Testing

Consider having your deer tested, even if it's not mandatory in your hunting zone. Consider not eating your deer meat until CWD test results are determined to be "not detected."
https://www.dnr.state.mn.us/cwd/testing.html

Disinfection

CWD prions can be removed from stainless steel surfaces (i.e., knife blades, processing tables, etc.) by using a 1:1 water to household bleach solution and a 5 minute soak. Always follow the appropriate safety precautions when handling bleach.

Funding for this project was provided by the Minnesota Environment and Natural Resource Trust Fund as recommended by the Legislative-Citizen Commission on Minnesota Resources (LCCMR).




Chronic Wasting Disease

"Deer are one of the very important animals within our ecosystem here...it's a part of the wildlife community here." - Grand Portage community member

Introduction

For many, deer hunting is a "way of life." Across many generations, deer have been important members of the wildlife community, providing a vital food source and bringing families and communities together through sharing of meat, culture, and traditions. To the concern of many communities, chronic wasting disease (CWD) is spreading in our region. It is caused by malfunctioning prions, which infect deer, and it always results in death. CWD could make many deer sick, reduce the number of wild deer, and threaten hunting and cultural activities. However, we can all help slow the spread of the disease by learning more about it: how it spreads and the actions we can take to prevent its further spread.

We sincerely thank Michael Waasegiizhig Price (Wikwemikong First Nations), Dylan Bizhikiins Jennings, and Kelly Applegate for lending their opinion and experiences to earlier versions of this illustration.
Illustration by: Sequential Potential LLC,
Twitter @s_p_comics
Artist: Alex D. Araiza
Designed by: Ellen E. Brandell &
Marie L.J. Gilbertson
Funded by: AGU, Sharing Science Grants for Science Communication and Outreach

What is a prion?

A prion (pronounced *PREE-on*) is a protein present in all mammals that help cells in the body to function normally. When normal prion proteins misfold, they lose this ability and cause disease. Abnormally folded prion proteins can cause normally folded and functioning prions to misfold. Over time, as the misfolded proteins bind together and accumulate, they cause the destruction of brain cells and signs of illness develop. This eventually leads to death.

Prions cause a variety of fatal disorders in humans and animals. These include scrapie in sheep and goats, bovine spongiform encephalopathy (BSE or mad cow disease) in cattle, and chronic wasting disease (CWD) in cervids (i.e., deer). White tailed deer, mule deer, black tailed deer, elk, and moose are known to be susceptible to CWD. Creutzfeldt-Jakob disease, Alzheimer's, Parkinson's, and amyotrophic lateral sclerosis (ALS) are examples of prion diseases that affect humans.

How is CWD spread?

The transmission of CWD is varied and complex. CWD-causing prions are present throughout an infected deer: in blood, saliva, semen, urine, feces, antler velvet, muscle and other tissues. Thus, as an infected deer lives on, it can shed CWD-causing prions into the environment through its saliva, urine, and other bodily fluids; infected does can even pass CWD prions on to their fawns before birth. Once the infected animal dies, prions can be released into the environment from the carcass of the animal. The unique shape of CWD prions makes them resistant to degradation and destruction; they can remain infectious in the environment even after many years. We know that healthy deer can become infected when they interact with infected deer or from the environment when it is contaminated by CWD prions.

How can I tell if a deer has CWD?

Deer that are infected with CWD can appear healthy and normal for a very long time. It can take up to two years for signs of disease to appear, and this is generally only in the final few months. Sick deer might show signs of drinking and urinating more than normal, incoordination, drooling, loss of fear of humans, unusual social interactions with other deer, poor hair coat and loss of body condition (i.e., they become skinny).

Is venison safe to eat?

There is currently no evidence that humans have contracted a prion disease from consuming meat from a deer with CWD, but there is some concern for this. Like viruses, CWD prions can change as they infect new deer, and those changes can result in new strains. Because it is very difficult to identify strains of CWD and how they might differ in their risk to people, the general recommendation is that people not eat venison from deer that have CWD.

What can I do to safely process a deer if CWD is in my area?

CWD prions have not been shown to cause human disease, however, public health officials and natural resource managers recommend certain steps that can reduce the risk of spreading the disease.

- Wear latex gloves while field dressing and processing your deer. When processing your deer, remove any lymph nodes that you see (see the end of this document for more information about lymph nodes). Butcher and process your own venison. However, if you use the services of a commercial or private processor, consider having them process and wrap your meat individually, so as not to be mixed with the meat of other deer.
- Use stainless steel tools and surfaces, and clean them with a 1:1 water to household bleach solution and a 5-minute soak.
- Get your harvest sampled and tested for CWD before consuming the venison.
- If you hunt in an area where CWD might be present, follow state, local and tribal laws related to carcass transport and disposal.

How is a deer harvest tested for CWD?

Lymph nodes from the head (retropharyngeal lymph nodes) are typically collected by natural resource agencies conducting testing at the time of harvest. These tissues are then sent to a laboratory that determines if the lymph nodes have any evidence of prions in them. Check with your tribal or state natural resource agencies to determine if CWD testing is required or recommended for the area where you hunt; they will also have information on where and how to get your deer sampled for testing.

Why is CWD testing important?

CWD has been discovered in new locations in recent years. Whether you harvest a deer in an area known to have CWD or not, it is important to have the animal tested for CWD before consuming the meat. CWD testing gives natural resource managers a better understanding of where CWD is in the state. That information helps managers make decisions on how to keep infection levels among deer at low levels, which benefits the health of the population and reduces any risks to humans.

What else can I do?

Report any sick deer to your local tribal Natural Resource Department or state Department of Natural Resources.

Know the regulations where you hunt.

Get your harvested deer tested for CWD.

Keep hunting, but hunt responsibly! We should all protect the health of our deer and environment.

Where can I find more information?

Here are just a few additional resources:

For hunting regulations in your state: https://cwd-info.org/cwd-hunting-regulations-map/

For an educational video series about CWD, search for the MSU Deer Lab CWD Series on YouTube, or type this link into your browser: https://www.youtube.com/watch?v=KA3k3LJ1Cg8

For a video demonstration of how to identify and remove lymph nodes, go to https://mnpro.umn.edu and click on Outreach Resources at the top of the page. From there, scroll down to find the lymph node sampling video, or type the following link into your browser: https://www.youtube.com/watch?v=5M_9FXp9Zuo

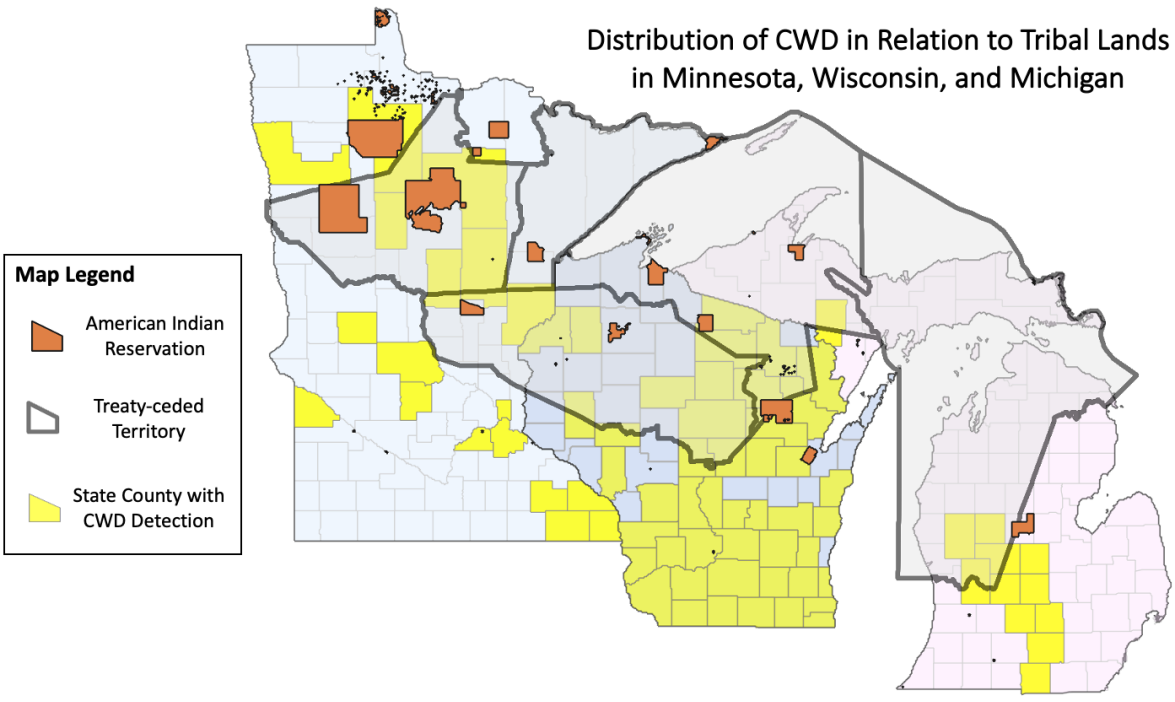

scientific reports

Check for updates

OPEN

RT-QuIC detection of CWD prion seeding activity in white-tailed deer muscle tissues

Manci Li[1,2], Marc D. Schwabenlander[1,2], Gage R. Rowden[1,2], Jeremy M. Schefers[2,3], Christopher S. Jennelle[4], Michelle Carstensen[4], Davis Seelig[2,5] & Peter A. Larsen[1,2]✉

Chronic wasting disease (CWD) is a prion disease circulating in wild and farmed cervid populations throughout North America (United States and Canada), Europe (Finland, Norway, Sweden), and South Korea. CWD is a long-term threat to all cervid populations and to cervid hunting heritage, with the potential to cause substantial economic losses across multiple sectors. In North America, hunting and farming industries focused on the processing and consumption of white-tailed deer (WTD) venison are particularly vulnerable to CWD prion contamination, as millions of WTD are consumed annually. Real-time quaking-induced conversion (RT-QuIC) is a highly sensitive assay amplifying misfolded CWD prions in vitro and has facilitated CWD prion detection in a variety of tissues and excreta. To date, no study has comprehensively examined CWD prion content across bulk skeletal muscle tissues harvested from individual CWD infected WTD. Here, we use RT-QuIC to characterize prion-seeding activity in a variety of skeletal muscles from both wild and farmed CWD-positive WTD. We successfully detected CWD prions in muscles commonly used for consumption (e.g., backstrap, tenderloin, etc.) as well as within tongue and neck samples of WTD. Our results suggest that CWD prions are distributed across the skeletal muscles of infected WTD. We posit that RT-QuIC will be a useful tool for monitoring CWD prions in venison and that the method (with additional protocol optimization and high-throughput functionality) could be used to reduce and/or prevent CWD prions from entering animal and human food chains.

Chronic wasting disease (CWD) is an infectious and fatal prion disease transmitted among cervids, including white-tailed deer (WTD; *Odocoileus virginianus*), mule deer, elk, red deer, caribou, reindeer, and moose. The disease is a direct threat to a number of cervid-related multibillion-dollar economic sectors, including both agricultural and hunting industries, and it is now prevalent in the USA and Canada with additional cases in Korea, and Scandinavian regions[1]. As with other transmissible spongiform encephalopathies[2,3], CWD prion seeds (PrP^{CWD}) consist of misfolded cellular prion protein (PrP^{C}) which form β-sheet-rich amyloid fibrils through inducing conformational change and polymerization of native PrP^{C}. The central nervous system (CNS) typically contains the highest load of prions in a terminally diseased animal in comparison to peripheral tissues and body excreta due to the abundance of PrP^{C} in nervous tissues[4].

Recent studies have shown that there are compelling reasons to suggest that CWD poses a non-zero risk to a variety of mammals, including humans[1,5]. Challenge experiments using CWD prions have shown that CWD can cause neurodegenerative disease in numerous species, including ferrets, mink, domestic cats, sheep, goats, cows, pigs, and squirrel monkeys[6]. In vitro experiments showed that CWD prions can convert human prion proteins into a misfolded and potentially disease-causing form[5]. For these reasons, as of 2020, both the Food and Drug Administration (FDA) and Food Safety and Inspection Service, United States Department of Agriculture (FSIS, USDA) consider venison from CWD-positive animals as adulterated and unsuitable for consumption[7,8]. While there is no evidence of CWD transmission to humans[1], the National Institutes of Health and Centers for Disease Control and Prevention suggests that people should not consume known CWD-infected venison.

[1]Department of Veterinary and Biomedical Sciences, University of Minnesota, 1971 Commonwealth Ave, Saint Paul, MN 55108, USA. [2]Minnesota Center for Prion Research and Outreach, College of Veterinary Medicine, University of Minnesota, Saint Paul, MN 55108, USA. [3]Veterinary Diagnostic Laboratory, Veterinary Population Medicine Department, University of Minnesota, Saint Paul, MN 55108, USA. [4]Minnesota Department of Natural Resources, 5463 West Broadway, Forest Lake, MN 55025, USA. [5]Department of Veterinary Clinical Sciences, University of Minnesota, Saint Paul, MN 55108, USA. ✉email: plarsen@umn.edu

Currently, CWD diagnosis relies on the identification of Proteinase K (PK)-resistant PrP^{CWD} by enzyme-linked immunosorbent assay (ELISA) and immunohistochemistry (IHC)[9]. These standardized methods for detecting CWD are designed to have consistent protocols with quantified estimates of test accuracy that are scalable to meet the needs of agencies conducting surveillance and monitoring to manage the disease. However, there are limitations to the existing antibody-based diagnostic approaches, namely relatively poor sensitivity as well as the inability to screen biofluids and environmental samples. In the past two decades, the detection of prion seeding activity has been greatly enhanced by highly sensitive methods involving amplification of protein misfolding in vitro, such as protein misfolding cyclic amplification (PMCA) and real-time quaking-induced conversion (RT-QuIC)[9,10]. PMCA uses rodent brain homogenates as the substrate to amplify misfolded prions and Western Blotting as the output[9,11,12]. RT-QuIC utilizes recombinant PrP^{C}, commonly from rodent sources, as the substrate for prion amyloid formation, the real-time reporting of which is enabled by thioflavin T (ThT) binding and detection[13–15]. Although RT-QuIC demonstrates unparalleled detection sensitivity and specificity for brain and lymphoid tissues, it has lower sensitivity for other sample types; this has in-part been ascribed to lower prion density and RT-QuIC reaction inhibitors[16]. Importantly, the inhibitory effect of certain tissues—likely due to their biochemical compositions[16,17], such as blood[18–20] and saliva, seemed to be specific for RT-QuIC but not PMCA[16]. Dilutions (diluting out inhibitory effects) and phosphotungstic acid (PTA) precipitation are commonly used to increase RT-QuIC sensitivity by enriching for prions and overcoming effects of RT-QuIC inhibitors[15–17,20], although other methods exist[18,21].

CWD prions have previously been identified in a variety of tissue types and excreta using RT-QuIC, such as the CNS, third eyelids, and feces[22–25]. Prior studies focused on the detection of CWD prions in skeletal muscle using immunodetection methods have produced mixed results[26–29]. PMCA was used to amplify CWD prions in hindlimb muscles from two WTD[30]. Skeletal muscle tissues from CWD-infected deer contain infectious prions as determined in transgenic mice bioassay[29]. Despite clear advantages of RT-QuIC as a screening method[9,31,32], no comprehensive reports are available for detecting CWD prions using RT-QuIC in skeletal muscle.

Cervid skeletal muscles are consumed by a growing population of hunters and restaurant clientele and have become a common ingredient in pet food (e.g., commercial cat and dog food). At the time of this publication, there are no guidelines regarding venison-based detection of CWD and associated food-product surveillance. This observation, combined with the limitations of existing CWD diagnostic tools (e.g., ELISA and IHC), has resulted in a situation whereby venison processing can occur without the knowledge of an animal's CWD status, and it is estimated that at least 15,000 CWD positive cervids are consumed in the USA annually[1]. Underscoring this statistic was a well-documented 2005 exposure event in which over 200 participants at a Sportsmen's feast consumed CWD-positive venison[33]. Current estimates indicate a 20–50% CWD prevalence rate in harvested WTD from focal areas of southern Wisconsin, however, only 1 out of 3 are tested for the disease[33]. Collectively, these observations highlight the need for post-harvest production-level monitoring of cervid products used for human and animal consumption.

Here, we examine the utility of RT-QuIC for the detection of CWD prions within a broad set of WTD skeletal muscle tissues, including those frequently used for both human and animal consumption. We report the RT-QuIC results for muscles sampled from the neck (*brachiocephalicus/sternocephalicus*) of wild WTD with known CWD status. Further, we investigated whether CWD prion deposition is limited to certain groups of muscles or if it is more generalized by using multiple WTD skeletal muscle groups across the body, including muscles from the tongue, forelimb (*suprascapularis*), backstrap (*longissimus dorsi*), tenderloin (*psoas major*), and hindlimb (*semimembranosus/semitendinosus*) from both wild and farmed CWD positive animals independently determined by ELISA and/or IHC.

Results

RT-QuIC detection of CWD prions in unilateral skeletal muscles from the neck of wild WTD. We first developed a PrP^{CWD} enrichment protocol for muscles—based on previous work[20,25]—herein referred to as the freeze–thaw method as it consists of several rapid freeze–thaw cycles prior to PTA precipitation. To test the performance of the freeze–thaw method, we processed unilateral muscles collected from the neck (*brachiocephalicus/sternocephalicus*) of 10 CWD-positive and 10 CWD-negative wild WTD (Table 1) and analyzed the resultant homogenates using RT-QuIC. We found that we could detect significant prion seeding activity in 8 out of 10 (80%) samples from 10 different CWD-positive animals (Table 1; Fig. 1a) with relatively consistent fluorescent readings (Fig. 1b). In contrast to animals with official CWD-positive test results (i.e., ELISA and IHC), none of the muscle samples from CWD-negative animals showed statistically significant prion seeding activity in RT-QuIC (Fig. 1b), despite one of eight wells crossing the threshold from a single animal (Fig. 1d).

We then compared the rate of amyloid formation (RAF) among muscles, blood, and lymphoid tissues, all of which were processed using mechanical extraction methods; with methods and results of blood and lymphoid tissues reported by Schwabenlander et al.[32]. We note that although muscles appeared to have a lower RAF, it is possible for an animal to have a statistically positive RT-QuIC result for muscles and lymphoid tissues but not blood (e.g., animal 166; Fig. 2a; see Schwabenlander et al. In press). 1:10 dilution of the enriched homogenates (after NaPTA precipitation) was chosen because of its consistency in producing results in different animals (Fig. 2b). The optimal dilutions (a log10-based dilution that would produce the highest RAF for a given sample) of each animal may differ, with dilution factors ranging from 0 to 3 (Fig. 2b). Because the initial concentration of prion seeds added into RT-QuIC reaction is known to affect detectability and RAF[15], it is then expected that the method presented here—using suboptimal dilutions for some samples—would underestimate the RAF for consistent detection purposes. Indeed, by comparing the RAF between 1:10 dilution of the enriched homogenates and lymphoid tissues, which exhibit RAF 10 times lower than brain homogenates[17], we found that indirectly calculated brain/muscle ratio was 100–1000 times lower than previously reported in muscles of mice inoculated

MNPRO ID	ELISA/IHC CWD test result	RT-QuIC result	RT-QuIC wells positive
166	+	***	7/8
250	+	**	6/8
333	+	**	6/8
353	+	*	5/8
360	+	****	8/8
363	+	*	5/8
376	+	***	7/8
384	+	***	7/8
508	+	NS	2/8
735	+	NS	1/8
443	–	–	0/8
239	–	–	0/8
515	–	–	0/8
536	–	–	0/8
693	–	NS	1/8
708	–	–	0/8
723	–	–	0/8
727	–	–	0/8
734	–	–	0/8
762	–	–	0/8

Table 1. RT-QuIC results of WTD neck muscles. All animals were collected through the Minnesota Department of Natural Resources 2019 agency culling operations. All animals' medial retropharyngeal lymph nodes were tested for CWD through official regulatory means by ELISA, with IHC confirmation on ELISA positives. Mann–Whitney U test: NS, rate of amyloid formation is not 0 but not statistically significant from the corresponding negative controls; –, rate of amyloid formation is 0 in the given time period; ****$p < 0.0001$; ***$p < 0.001$; **$p < 0.01$; *$p < 0.05$. The freeze–thaw method was used for sample processing and RT-QuIC was performed at 45 °C.

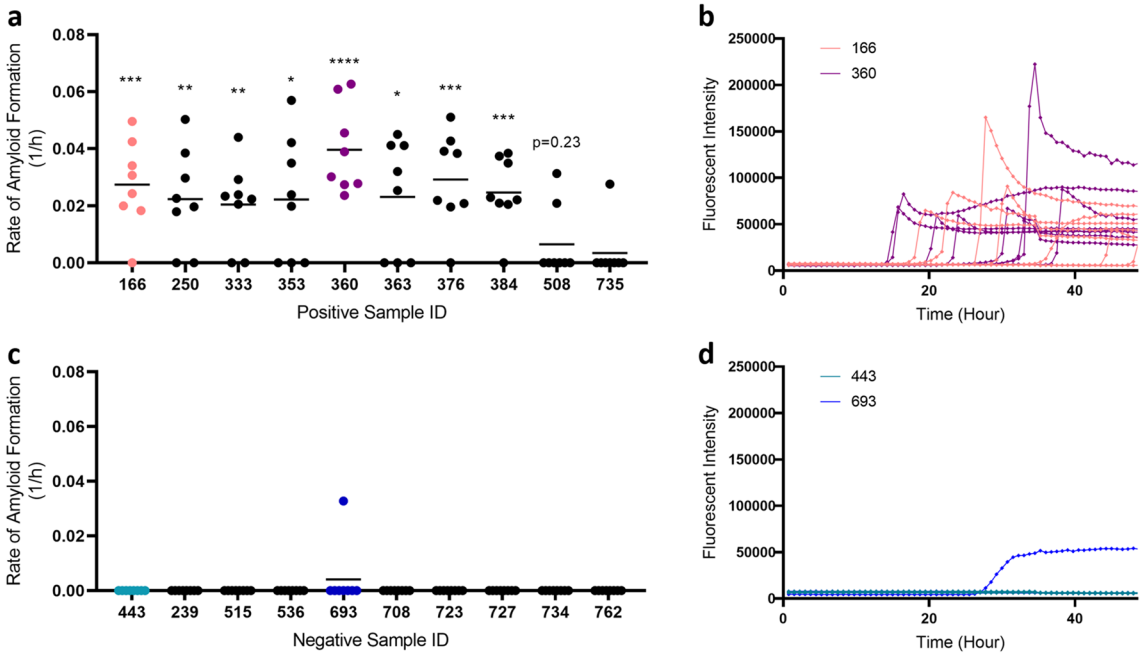

Figure 1. Detection of prion seeding activity in unilateral neck muscles from white-tailed deer. (**a**) Rate of amyloid formation (1/h) was plotted using data collected from CWD-positive animals. Statistical significance was obtained through comparing with rate of amyloid formation with the respective negative controls on the same plate (****$p < 0.0001$; ***$p < 0.001$; **$p < 0.01$; *$p < 0.05$). (**b**) Examples of real-time fluorescence readings from positive animals (sample IDs 166 and 360). (**c**) Rate of amyloid formation (1/h) from CWD-negative animals. (**d**) Examples of real-time fluorescence readings from negative animals (443 and 693); plotted as described in (**b**) and showing one of eight wells for sample 693 having amyloid seeding activity (not significant).

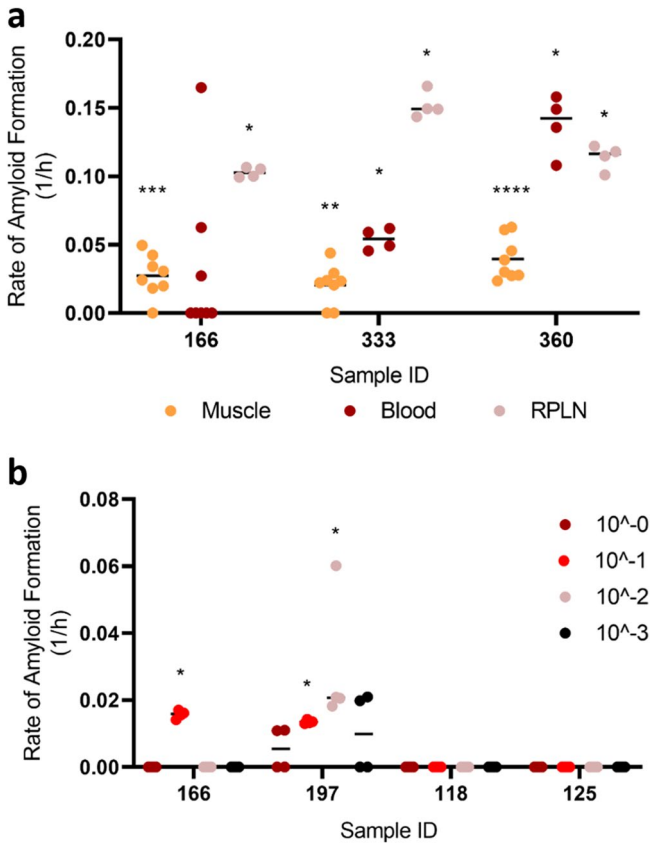

Figure 2. Comparison of prion-seeding activity in RT-QuIC. (**a**) Rate of amyloid formation was compared among neck muscle, blood, and lymphoid tissues of three CWD-positive animals. (**b**) Rate of amyloid formation compared between each sample and the negative control on the same plate. Statistical result for each sample compared with its respective negative control was indicated (****$p < 0.0001$; ***$p < 0.001$; **$p < 0.01$; *$p < 0.05$). RPLN, medial retropharyngeal lymph nodes.

with different strains of prions (Supplementary Fig. 1)[34]. Because the tenfold dilution for each sample was likely not optimal, the difference could be attributed to a combination of the presence of RT-QuIC inhibitors in muscle tissues and incomplete extraction (Bosque et al. pulverized muscles under liquid nitrogen[34]) in addition to experimental design and species differences. It is also possible that particular CWD prion seeds within our samples were partially degraded during autolysis (discussed further below).

CWD prions found in muscles from the tongue, neck, mid-trunk, forelimb, and hindlimb of WTD. To investigate if the CWD prions are found in WTD skeletal muscles and whether the freeze–thaw method described above can be used to detect prions deposition in other skeletal muscles other than those from the neck, we used a set of muscle tissues from another 10 WTD, including the tongue, forelimb (*suprascapularis*), backstrap (*longissimus dorsi*), tenderloin (*psoas major*), and hindlimb (*semimembranosus/semitendinosus*). In the blinded run, we were able to detect at least one significantly RT-QuIC positive sample in all the muscle groups tested (Table 2; Fig. 3). We observed poor sensitivity of the freeze–thaw method with these particular samples (Table 2; when compared to fresh samples), a result that is likely due to the deteriorated condition of the muscle tissues upon receipt. Nevertheless, we recovered statistically significant RT-QuIC results for a variety of muscle groups and we therefore conclude that PrP^{CWD} occurs broadly throughout the skeletal muscles of infected WTD (Fig. 3b) and are not limited to specific muscle groups, as previously reported in mouse models[34].

Notably, the samples used for this experiment were undergoing various degrees of autolysis. Hypothesizing that this may influence RT-QuIC's ability to detect prion-seeding activity by changing the optimal dilutions of the processed homogenate, we again looked at prion-seeding activities using serial dilutions of a selected number of samples. As expected, the dilution with adequate positive wells for samples no longer consistently converged at 10^{-1} (Fig. 4a), suggesting that the freeze–thaw method is not suitable for muscle tissue samples of sub-optimal quality. To investigate whether other tissue processing methods would improve the detection of CWD prion-seeding activity in RT-QuIC, given the sub-optimal tissue preservation described above, we examined a subset of samples using enzymatic digestions (collagenase A and trypsin) instead of the freeze–thaw method. We hypothesized that collagenase A and/or trypsin would sufficiently digest potential inhibitors and/or further "release" CWD prions to a degree where extensive dilution of the processed homogenates was unnecessary. Surprisingly, collagenase A digestion still required a tenfold dilution similar to the freeze–thaw method (Supplementary

ID	Region	MNPRO ID	ELISA and/or IHC CWD test result	RT-QuIC result	RT-QuIC wells positive
1	F	287	+	–	0/8
2	H	287	+	NS	3/8
3	Tg	287	+	***	8/8
4	B	287	+	–	0/8
5	F	288	+	NS	1/8
6	H	288	+	NS	1/8
7	B	288	+	NS	1/8
8	F	289	+	NS	1/8
9	H	289	+	–	0/8
10	B	289	+	–	0/8
11	F	290	+	–	0/8
12	H	290	+	NS	2/8
13	Tg	290	+	–	0/8
14	Td	290	+	–	0/8
15	H	295	+	NS	1/8
16	F	295	+	–	0/8
17	B	295	+	NS	1/8
18	H	296	+	–	0/8
19	F	296	+	–	0/8
20	B	296	+	–	0/8
21	H	297	+	NS	1/8
22	F	297	+	NS	1/8
23	B	297	+	–	0/8
24	H	298	+	NS	1/8
25	F	298	+	–	0/8
26	B	298	+	–	0/8
27	H	307	+	***	8/8
28	F	307	+	****	8/8
29	B	307	+	*	4/8
30	Td	307	+	NS	1/8
31	H	311	+	–	0/8
32	F	311	+	–	0/8
33	B	311	+	–	0/8
34	Td	311	+	*	5/8

Table 2. RT-QuIC results of various WTD muscle groups. All animals' medial retropharyngeal lymph nodes were tested for CWD through official regulatory means by ELISA, with IHC confirmation on ELISA positives, except MNPRO ID 307, which was tested by IHC only on obex and medial retropharyngeal lymph nodes. Mann–Whitney U test: NS, rate of amyloid formation is not 0 but not statistically significant from the corresponding negative controls; –, rate of amyloid formation is 0 in the given time period; ****$p < 0.0001$; ***$p < 0.001$; **$p < 0.01$; *$p < 0.05$. RT-QuIC analyses of the forelimb (F), hindlimb (H), backstrap (B), tenderloin (Td), and tongue (Tg) muscles were performed with the researcher blinded to official CWD testing results (see methods). The freeze–thaw method was used for sample processing and RT-QuIC was performed at 45 °C.

Fig. 2) although it appeared to be more sensitive [i.e., identified more muscle samples as RT-QuIC positive from CWD positive animals (Fig. 4b)]; however, this was not observed when we re-tested a subset of neck muscle samples. In addition, we confirmed that the collagenase method did not appear to produce false-positive RT-QuIC signals (Supplementary Fig. 3). Alternatively, trypsin digestion produced an extremely high RAF without requiring the tenfold dilution even though its sensitivity did not improve upon the freeze–thaw method in the given sample set (Fig. 4c).

We note that all methods used in this study did result in positive prion-seeding activities using RT-QuIC on muscle tissue (Fig. 4b). The results reported here indicate that the freeze–thaw method may not be enough to facilitate RT-QuIC detection of CWD prions in aged or decomposing muscles but has utility for freshly collected samples.

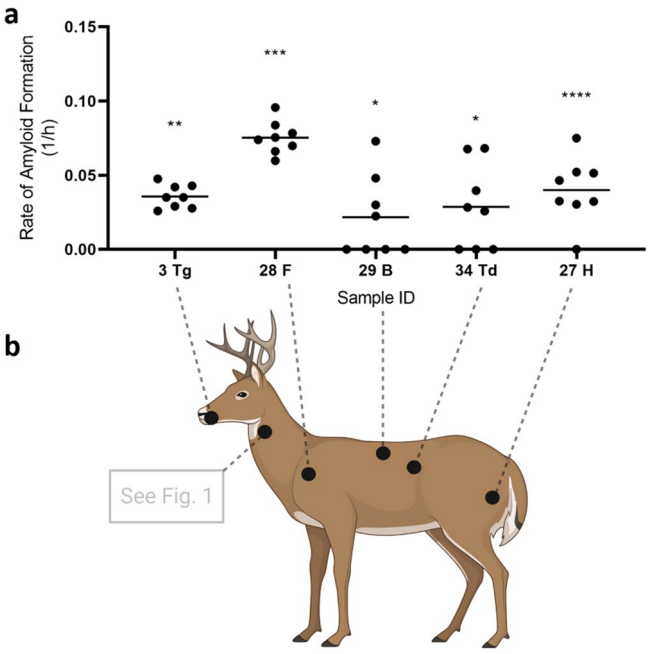

Figure 3. Presence of CWD prions in the muscle tissues of tongue, neck, hindlimb, forelimb, backstrap, and tenderloin. (**a**) Examples of the rate of amyloid formation (RAF) from RT-QuIC positive samples were plotted. Statistical results as compared to the respective negative controls were indicated (****$p < 0.0001$; ***$p < 0.001$; **$p < 0.01$; *$p < 0.05$). *Tg* Tongue, *F* forelimb, *B* backstrap, *Td* tenderloin, *H* hindlimb. Numbers on X-axis are animal IDs listed in Table 2. (**b**) Prion-seeding activity was detected by RT-QuIC in muscles from the tongue, forelimb, backstrap, tenderloin, and hindlimb. Deer image was created using BioRender.com.

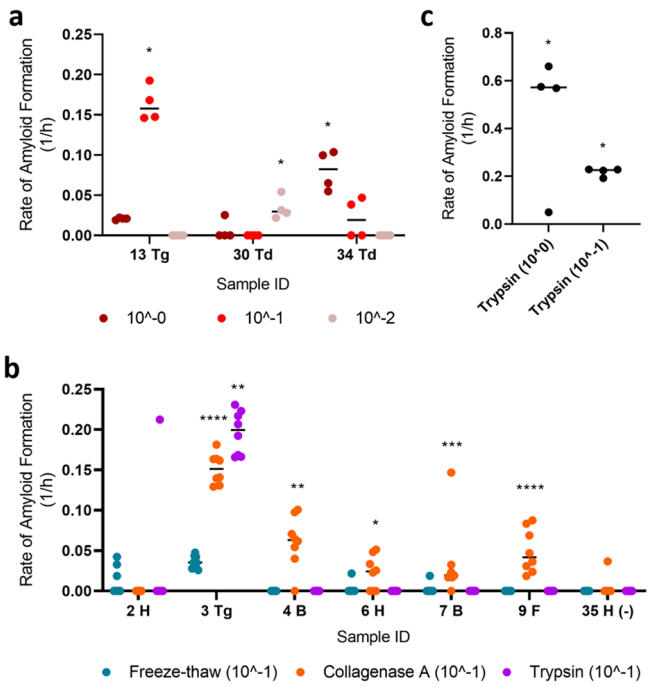

Figure 4. Comparison of different methods used to extract CWD prions from skeletal muscles of WTD. (**a**) Rate of amyloid formation (RAF) of samples diluted to different concentrations was visualized. (**b**) RAF from RT-QuIC was plotted for a subset of samples treated by different extraction methods, including freeze–thaw, collagenase A, and trypsin. The final suspension was diluted to 10^{-1}. (**c**) RAF of trypsin-digested sample number 3 (tongue; undiluted and diluted to 10^{-1}) was diagramed. Statistical result for each sample when compared with its respective negative control was indicated (****$p < 0.0001$; ***$p < 0.001$; **$p < 0.01$; *$p < 0.05$). *B* backstrap, *F* forelimb, *H* hindlimb, *Td* tenderloin, *Tg* tongue.

Discussion

CWD is an emerging infectious prion disease currently affecting cervid populations across three continents and negatively influencing all cervid-related industries within impacted regions. Infected animals can remain asymptomatic for months while shedding CWD prions through excreta[22,25], thus making the identification of early-stage CWD-infected animals based on external diseased phenotypes impossible. Antibody-based ELISA and IHC tests are the current diagnostic standards for CWD. Despite their reliability, such immunodetection methods have limited sensitivity and application across various tissues and body excreta in comparison to in vitro amplification methods for prion detection, such as PMCA and RT-QuIC[9]. Of the available in vitro amplification methods, RT-QuIC is well-suited as a CWD screening tool because it can be easily scaled up as required by industrial applications. Given the continued spread of CWD, and uncertainty surrounding potential health risks to both animals and humans due to the consumption of CWD-positive venison[1], it is clear that a highly sensitive and reliable diagnostic method to detect CWD prions in skeletal muscles of cervids is needed.

In this study, we tested methods aimed at extracting and enriching PrP^{CWD} from WTD skeletal muscles for prion detection by RT-QuIC. We first found that CWD prions were present in bulk sampled neck muscles (*brachiocephalicus*/*sternocephalicus*) of CWD positive animals (Fig. 1a)[32]. This result prompted us to investigate the general distribution of prions in skeletal muscles from the tongue, forelimb, mid-truck, and hindlimb of CWD positive WTD tissue-sets available in our biorepository. We found that in addition to the neck, PrP^{CWD} is also present in a variety of skeletal muscle tissues (described above; Table 2; Fig. 3). Our results, based on a sampling of various muscle groups, suggest that CWD prions are distributed across CWD infected WTD skeletal muscles. Additional research is needed to determine the full extent to which CWD prions occur within particular muscle tissue types of infected animals, including intra- and inter-individual variation of CWD prion accumulation in WTD muscles.

It remains to be determined whether CWD prions are detectable in skeletal muscles that were not sampled herein or in similar studies using amplification-based methods, such as PMCA and RT-QuIC. Although we were unable to detect PrP^{CWD} across all muscle types within a given CWD positive animal, this result is expected because the successful detection of PrP^{CWD} within an infected individual, and particular tissue type, can be impacted by multiple factors. With respect to the neck samples screened here, we only had access to unilaterally sampled muscles harvested from individual WTD heads and it has been shown recently that PrP^{CWD} may not be bilaterally present in select tissues[32,35]. The 10 positive animals (originating from wild WTD herds) selected for testing of neck muscles were strongly positive across multiple tissues and likely were in relatively advanced, yet pre-clinical stages of the disease (i.e., no clinical signs were observed at the time of euthanasia)[32]. The stability of prions may vary depending on strains[36] and, to date, no RT-QuIC method is available to detect particular CWD strain differences. Further, the progression of CWD affects the deposition of prions in peripheral tissues and it is unclear at what time in the disease progression that prions accumulate in WTD muscles. We note the neck muscles used herein were frozen less than 12 h after collection; however, the other muscle tissues were at various stages of decomposition and underwent multiple freeze–thaw cycles prior to our possession. This difference in tissue preservation and quality potentially accounts for the reduced sensitivity of RT-QuIC upon application, an observation that suggests an altered balance of RT-QuIC inhibitors and active prion seeds and/or degradation of particular CWD prion strains in decaying tissue. Thus, we recommend muscles for RT-QuIC-based analyses of CWD prions be frozen (at either −20 °C or −80 °C) as soon as possible after collection, ideally less than 24 h.

Based on the results from well-preserved neck muscles, we posit that the freeze–thaw method has the most potential for large-scale diagnostic screening of venison, as it is cheaper and easier to perform. For samples with heavy prion loads, such as tongue, all methods used in this study agreed on the positivity of prion-seeding activity. For poorly preserved sample types, collagenase A outperformed the freeze–thaw method and trypsin digestion in terms of identifying more RT-QuIC positive muscle samples from CWD positive animals. Surprisingly, trypsin digestion yielded a high RAF and did not require additional dilutions of the final resuspension as needed by other methods. This could be due to the digestion of protein inhibitors by trypsin and/or superior ability of trypsin to free prions from examined tissues. Additional optimization of the methods presented here is needed for protocols focused on suboptimal sample types. It is possible that the prion seeding activity we detected in the collected muscle tissues is from non-muscle cell types as reported by Daus et al.[28]. However, the cellular origin of PrP^{CWD} in skeletal muscle, whether in myocytes, erythrocytes, neurons, epithelial cells, or any other cell type, is inconsequential to the recommendations of not consuming venison from CWD-positive animals or the potential for RT-QuIC-based venison screening as venison products are a matrix of multiple tissues and cell types.

Our findings suggest that CWD prions occur throughout an array of WTD muscles and further investigation, from an anatomical perspective, is needed to understand the extent of this distribution. Future studies focusing on larger sample sizes with systematic, bilateral samplings of well-preserved muscle samples throughout the body are needed to assess, validate, and improve the presented method for its application, as well as quantify the load of CWD prions present. Longitudinal characterization of prion deposition (i.e., using cervid challenge experiments) in a variety of high-quality muscle samples, such as those conducted for saliva, lymphoid tissues, and feces is needed to better understand the pathophysiology of CWD in deer and other cervids. Our study provides the foundation for the development of RT-QuIC-based screening of venison and venison-related products associated with food processing pipelines for CWD-prions.

Methods

Experimental design. The RT-QuIC muscle protocols (freeze–thaw and enzymatic digestion, detailed below) were initially used on a small subset of CWD positive and not-detected neck muscle tissue samples. After refining our methods, we then tested the protocol on a larger set of neck muscles from ten CWD positive and ten CWD not detected deer, with CWD status determined by ELISA, IHC, and RT-QuIC analyses on lymphoid

tissues from the animals reported by Schwabenlander et al.[32]. To blind investigators, researcher "A" subsampled approximately 300 mg of each sample, placed them individually in 1.5 ml tubes, and re-labeled them in a randomized numerical order. Researcher "B" carried out the muscle processing and RT-QuIC and was blinded to the original identity of the samples. ELISA and IHC results for animals examined herein are presented in Supplementary Table 1. Researcher "B" was unblinded after the first pass of all samples; investigation of different extraction methods was done after unblinding.

Sample collection. RT-QuIC protocol development was initially performed utilizing neck muscle (*brachio cephalicus*/*sternocephalicus*) tissue samples collected from wild WTD through 2019 agency culling operations in southeast Minnesota conducted by the Minnesota Department of Natural Resources in conjunction with USDA APHIS Wildlife Services as described by Schwabenlander et al.[32] (Table 1). Muscle tissue samples for the quantitative comparison study were obtained through disposal or necropsy of farmed and wild WTD at the University of Minnesota Veterinary Diagnostic Laboratory and were stored at − 20 °C. All farmed and wild WTD examined in our study have been independently tested through official regulatory means by the National Veterinary Services Laboratories or Colorado State University, respectively, for CWD infection based on immunodetection analysis (ELISA and/or IHC) of the brain and/or lymphatic tissue for the presence of PrP^{CWD} (Table 2).

Muscle preparation. *Freeze–thaw method.* This method was inspired by a combination of existing RT-QuIC protocols[20,25,28]. Muscles were stored at − 20 °C within 12 h after collection then transferred to − 80 °C until tested. 10% (weight/volume) muscle homogenates in 1× PBS were prepared in tubes with 1.5 mm diameter zirconium oxide beads using a Beadbug homogenizer at top speed for 180 s. The homogenates underwent three cycles of flash freeze–thaw consisting of 3 min in dry ice and 3 min at 37 °C. The homogenates were subjected to additional homogenization at top speed for 180 s using the Beadbug homogenizer. The mixtures were then centrifuged at 5000 rpm for 3 min. 500 µl of supernatants were used for centrifugation at 15,000 rpm, 4 °C for 40 min. The resultant pellets were resuspended in 100 µl of 1× PBS then incubated with 7 µl of 4% (w/v) phosphotungstic acid (Sigma-Aldrich) in 0.2 M magnesium chloride. The mixtures were then incubated at 37 °C and 1500 rpm for 1 h in a ThermoMixer (Eppendorf) before being subjected to centrifugation for 30 min at 15,000 rpm, 4 °C. Pellets were resuspended in 10 µl of 0.1% (v/v) SDS/PBS/N2. 2 µl of 10-1 diluted resuspension was used for optimal result.

Collagenase A and trypsin digestion method. This method for RT-QuIC was modified from the PMCA method developed by Daus et al.[28]. 10% (weight/volume, w/v) muscle homogenates and 180-s homogenization were carried out as described above. 350 µl homogenates were mixed with equal volume of 2× collagenase A [4 mM $CaCl_2$ and 0.5% (w/v), Roche] or trypsin (Gibco) solutions. The mixture was incubated at 37 °C, 700 rpm for four hours. After being homogenized again for 90 s, the mixtures were centrifuged at 5000 rpm for 3 min at 4 °C. The supernatant was then transferred to another tube and mixed with an equal volume of 2× protease inhibitor cocktail (Sigma-Aldrich). This was followed by steps including centrifugation at 15,000 rpm for 40 min as the freeze–thaw method. 2 µl of the final suspensions were diluted tenfold and added to the RT-QuIC reaction. The additional dilution was not necessary for trypsin digestion.

RT-QuIC substrate preparation and reaction conditions. Recombinant hamster PrP (HaPrP90-231; provided by NIH Rocky Mountain Laboratory) production and filtration followed the methods of Schwabenlander et al.[32]. All ingredients of RT-QuIC master mix (1× PBS, 500 µM EDTA, 50 µM ThT, 300 mM NaCl, and 0.1 mg/ml HaPrPrP) were filter-sterilized through 0.22 µm PVDF filters. 98 µL of the master mix was pipetted into wells of 96-well black clear bottoms plates. The plate was sealed with clear tape after 2 µL samples were added. Plates were then shaken on BMG FLUOstar Omega microplate readers (BMG LABTECH Inc., Cary, North Carolina, USA) at 700 rpm (57 s double orbital shaking followed by 83 s resting). Fluorescence was recorded after 21 shake/rest cycles using a 450 nm excitation filter and 480 nm emission filter. The gain was set to 1600. The machine performed 21 flashes/well and no well-scan was conducted. 45 °C, 50 °C, and 55 °C were used. 55 °C was only used for investigating whether decomposing tissues would have converging dilutions. 50 °C was used for enzymatic digestions.

Data analysis. Statistical analysis and plotting of fluorescence data from RT-QuIC were conducted using GraphPad Prism version 9.0 for Windows, GraphPad Software, San Diego, California USA, www.graphpad.com. RT-QuIC data from four or eight replicates were used for calculating the rate of amyloid formation (RAF) for muscles, which is defined by the inverse of the time to reach the fluorescent threshold[15]. The threshold was calculated as ten standard deviations above the average baseline fluorescence unless otherwise specified. We observed variable RAF values across the four microplate readers used for our analyses (i.e. plate reader one consistently exhibited earlier amyloid seeding rates vs. plate readers two, three, and four). In no instance did this impact our positive or negative controls. However, due to RAF differences among plate readers, this threshold could not be applied to all plates. In these rare circumstances, the threshold was calculated as two times the background fluorescence in each well. The differences in RAF calculated by these two methods for a true RT-QuIC positive sample is usually less than 0.01, therefore not influencing general comparisons of RAF among plates. The one-tailed Mann–Whitney unpaired u-test was used to test the average difference between samples and corresponding negative controls on the same plates. Quantitative analysis of CWD prion load in muscles was conducted as described by Henderson et al.[15].

Animal research statement. No white-tailed deer were euthanized specifically for the research conducted herein and all tissues were secured from dead animals or loaned for RT-QuIC analyses. For these reasons, the research activities conducted herein are exempt from review and approval by the University of Minnesota Institutional Animal Care and Use Committee (as specified https://research.umn.edu/units/iacuc/submit-maintain-protocols/overview). All CWD positive deer were submitted to the University of Minnesota College of Veterinary Medicine for disposal of infectious prions and were sampled prior to their disposal. White-tailed deer were euthanized by the Minnesota Department of Natural Resources (MN DNR) for annual culling efforts to control the spread of CWD in Minnesota following MN DNR state regulations and euthanasia guidelines established by the Animal Care and Use Committee of the American Society of Mammalogists[37]. All methods and all experimental procedures carried out during the course of this research followed University of Minnesota guidelines and regulations as approved by the Institutional Biosafety Committee under protocol #1912-37662H. This study was also carried out in compliance with the ARRIVE guidelines (https://arriveguidelines.org). We confirm that no human tissues were used for the research performed herein.

Field research. CWD negative animals were euthanized by the Minnesota Department of Natural Resources for routine annual culling efforts to control the spread of CWD in Minnesota and were not sampled specifically for the current study. Tissue samples were provided by the MN DNR.

Received: 17 May 2021; Accepted: 29 July 2021
Published online: 18 August 2021

References

1. Osterholm, M. T. *et al.* Chronic wasting disease in cervids: Implications for prion transmission to humans and other animal species. *MBio* **10**, e01091-e1119 (2019).
2. Prusiner, S. B. Novel proteinaceous infectious particles cause scrapie. *Science* **216**, 136–144 (1982).
3. Prusiner, S. B. Creutzfeldt-Jakob disease and scrapie prions. *Alzheimer Dis. Assoc. Disord.* **3**, 52–78 (1989).
4. Ford, M. J., Burton, L. J., Morris, R. J. & Hall, S. M. Selective expression of prion protein in peripheral tissues of the adult mouse. *Neuroscience* **113**, 177–192 (2002).
5. Barria, M., Libori, A., Mitchell, G. & Head, M. Susceptibility of human prion protein to conversion by chronic wasting disease prions. *Emerg. Infect. Dis. J.* **24**, 1482 (2018).
6. Hannaoui, S., Schatzl, H. M. & Gilch, S. Chronic wasting disease: Emerging prions and their potential risk. *PLoS Pathog.* **13**, e1006619 (2017).
7. FDA. Use of Material from Deer and Elk in Animal Feed. http://www.fda.gov/media/69936. Accessed 05 Feb 2021.
8. FSIS, USDA. Notice 16-20. Voluntary inspection of cervid animals tested for chronic wasting disease. (2020).
9. Haley, N. J. & Richt, J. A. Evolution of diagnostic tests for chronic wasting disease, a naturally occurring prion disease of cervids. *Pathogen (Basel, Switzerland)* **6**, 35 (2017).
10. Haley, N. J. *et al.* Management of chronic wasting disease in ranched elk: Conclusions from a longitudinal three-year study. *Prion* **14**, 76–87 (2020).
11. Kramm, C., Soto, P., Nichols, T. A. & Morales, R. Chronic wasting disease (CWD) prion detection in blood from pre-symptomatic white-tailed deer harboring PRNP polymorphic variants. *Sci. Rep.* **10**, 1–8 (2020).
12. Weber, P. *et al.* Cell-free formation of misfolded prion protein with authentic prion infectivity. *Proc. Natl. Acad. Sci.* **103**, 15818–15823 (2006).
13. Wilham, J. M. *et al.* Rapid end-point quantitation of prion seeding activity with sensitivity comparable to bioassays. *PLoS Pathog.* **6**, e1001217 (2010).
14. Atarashi, R., Sano, K., Satoh, K. & Nishida, N. Real-time quaking-induced conversion: A highly sensitive assay for prion detection. *Prion* **5**, 150–153 (2011).
15. Henderson, D. M. *et al.* Quantitative assessment of prion infectivity in tissues and body fluids by real-time quaking-induced conversion. *J. Gen. Virol.* **96**, 210–219 (2015).
16. Davenport, K. A., Hoover, C. E., Denkers, N. D., Mathiason, C. K. & Hoover, E. A. Modified protein misfolding cyclic amplification overcomes real-time quaking-induced conversion assay inhibitors in deer saliva to detect chronic wasting disease prions. *J. Clin. Microbiol.* **56**, e00947-18 (2018).
17. Clare, E. H., Kristen, A. D., Davin, M. H. & Mark, D. Z. Endogenous brain lipids inhibit prion amyloid formation in vitro. *J. Virol.* **91**, 1–12 (2017).
18. Orrù, C. D., Wilham, J. M., Vascellari, S., Hughson, A. G. & Caughey, B. New generation QuIC assays for prion seeding activity. *Prion* **6**, 147–152 (2012).
19. Abdel-Haq, H. Factors intrinsic and extrinsic to blood hamper the development of a routine blood test for human prion diseases. *J. Gen. Virol.* **96**, 479–493 (2015).
20. Elder, A. M. *et al.* Immediate and ongoing detection of prions in the blood of hamsters and deer following oral, nasal, or blood inoculations. *J. Virol.* **89**, 7421–7424 (2015).
21. Denkers, N. D., Henderson, D. M., Mathiason, C. K. & Hoover, E. A. Enhanced prion detection in biological samples by magnetic particle extraction and real-time quaking-induced conversion. *J. Gen. Virol.* **97**, 2023–2029 (2016).
22. Henderson, D. M. *et al.* Longitudinal detection of prion shedding in saliva and urine by chronic wasting disease-infected deer by real-time quaking-induced conversion. *J. Virol.* **89**, 9338–9347 (2015).
23. Hoover, C. E. *et al.* Pathways of prion spread during early chronic wasting disease in deer. *J. Virol.* **91**, e00077-17 (2017).
24. Cooper, S. K. *et al.* Detection of CWD in cervids by RT-QuIC assay of third eyelids. *PLoS One* **14**, e0221654 (2019).
25. Tennant, J. M. *et al.* Shedding and stability of CWD prion seeding activity in cervid feces. *PLoS One* **15**, e0227094 (2020).
26. Otero, A. *et al.* Prion protein polymorphisms associated with reduced CWD susceptibility limit peripheral PrP(CWD) deposition in orally infected white-tailed deer. *BMC Vet. Res.* **15**, 50 (2019).
27. Jewell, J. E., Brown, J., Kreeger, T. & Williams, E. S. Prion protein in cardiac muscle of elk (*Cervus elaphus nelsoni*) and white-tailed deer (*Odocoileus virginianus*) infected with chronic wasting disease. *J. Gen. Virol.* **87**, 3443–3450 (2006).
28. Daus, M. L. *et al.* Presence and seeding activity of pathological prion protein (PrPTSE) in skeletal muscles of white-tailed deer infected with chronic wasting disease. *PLoS One* **6**, 1–7 (2011).
29. Angers, R. C. *et al.* Prions in skeletal muscles of deer with chronic wasting disease. *Science* **311**, 1117 (2006).

30. Olszowy, K. M. *et al.* Six-year follow-up of a point-source exposure to CWD contaminated venison in an Upstate New York community: Risk behaviours and health outcomes 2005–2011. *Public Health* **128**, 860–868 (2014).
31. Haley, N. J. *et al.* Antemortem detection of chronic wasting disease prions in nasal brush collections and rectal biopsy specimens from white-tailed deer by real-time quaking-induced conversion. *J. Clin. Microbiol.* **54**, 1108–1116 (2016).
32. Schwabenlander, M. D. *et al.* Comparison of chronic wasting disease detection methods and procedures: Implications for free-ranging white-tailed deer (*Odocoileus Virginianus*) surveillance and management. *J. Wildl. Dis.* https://doi.org/10.1101/2021.03.03.433751 (2021) (**in press**).
33. Wisconsin Department of Natural Resources. Wisconsin Department of Natural Resources. https://dnr.wisconsin.gov/. Accessed 05 Feb 2021.
34. Bosque, P. J. *et al.* Prions in skeletal muscle. *Proc. Natl. Acad. Sci.* **99**, 3812–3817 (2002).
35. Bloodgood, J., Kiupel, M., Melotti, J. & Straka, K. Chronic wasting disease diagnostic discrepancies: The importance of testing both medial retropharyngeal lymph nodes. *J. Wildl. Dis.* **57**, 194–198 (2021).
36. Angers, R. C. *et al.* Prion strain mutation determined by prion protein conformational compatibility and primary structure. *Science* **328**, 1154–1158 (2010).
37. Sikes, R. S. & The Animal Care and Use Committee of the American Society of Mammalogists. 2016 Guidelines of the American Society of Mammalogists for the use of wild mammals in research and education. *J. Mammal.* **97**(3), 663–688 (2016).

Acknowledgements

We thank NIH Rocky Mountain Labs, especially Byron Caughey, Andrew Hughson, and Christina Orru for training and assistance with the implementation of RT-QuIC. We thank Fred Schendel, Tom Douville, and the staff of the University of Minnesota Biotechnology Resource Center for critical support with respect to the large-scale production of recombinant proteins. Evan Kipp and Suzanne Stone provided key assistance with laboratory techniques and logistics. We thank Lon Hebl for graciously providing access to animals housed at the Oxbow Park & Zollman Zoo. We are grateful to the following persons for their assistance with the collection of biological samples used herein: MNDNR Wildlife staff (especially Erik Hildebrand, Patrick Hagen, Kelsie LaSharr, and Margaret Dexter), Roxanne J. Larsen, Negin Goodarzi, Devender Kumar, the Minnesota Board of Animal Health, USDA APHIS Wildlife Services staff, and University of Minnesota Veterinary Diagnostic Lab Necropsy staff, especially Melissa Wolfe. The Minnesota Supercomputing Institute provided secure data storage of computational products stemming from our work. Funding was provided by the Minnesota State Legislature through the Minnesota Legislative-Citizen Commission on Minnesota Resources (LCCMR), Minnesota Agricultural Experiment Station Rapid Agricultural Response Fund, University of Minnesota Office of Vice President for Research, and start-up funds awarded to PAL through the Minnesota Agricultural, Research, Education, Extension and Technology Transfer (AGREETT) program. The Minnesota Department of Natural Resources provided funding for the staff needed to collect biological samples from wild deer and the costs for official CWD testing. Figure 3 was organized and partially created using BioRender (biorender.com).

Author contributions

M.L., M.D.S., D.S., and P.A.L. conceived of the study. M.L. designed the RT-QuIC experiments, collected data, and performed data analysis. M.L. and G.R.R. interpreted RT-QuIC results and prepared figures. M.L., M.D.S., D.S., and P.A.L. wrote the main manuscript. G.R.R., J.M.S., C.S.J., and M.C. helped to interpret results and write the manuscript. All authors reviewed the manuscript.

Funding

Funding was provided by the Minnesota State Legislature through the Minnesota Legislative-Citizen Commission on Minnesota Resources (LCCMR; awarded to PAL and DS), Minnesota Agricultural Experiment Station Rapid Agricultural Response Fund (awarded to PAL and DS), University of Minnesota Office of Vice President for Research (awarded to PAL), and start-up funds awarded to PAL through the Minnesota Agricultural, Research, Education, Extension and Technology Transfer (AGREETT) program. The funders had no role in study design, data collection and analysis, decision to publish, or preparation of the manuscript.

Competing interests

The authors declare no competing interests.

Additional information

Supplementary Information The online version contains supplementary material available at https://doi.org/10.1038/s41598-021-96127-8.

Correspondence and requests for materials should be addressed to P.A.L.

Reprints and permissions information is available at www.nature.com/reprints.

Publisher's note Springer Nature remains neutral with regard to jurisdictional claims in published maps and institutional affiliations.

scientific reports

Check for updates

OPEN

A field-deployable diagnostic assay for the visual detection of misfolded prions

Peter R. Christenson[1,2], Manci Li[2,3], Gage Rowden[2,3], Marc D. Schwabenlander[2,3], Tiffany M. Wolf[2,4], Sang-Hyun Oh[1,2]✉ & Peter A. Larsen[2,3]✉

Diagnostic tools for the detection of protein-misfolding diseases (i.e., proteopathies) are limited. Gold nanoparticles (AuNPs) facilitate sensitive diagnostic techniques via visual color change for the identification of a variety of targets. In parallel, recently developed quaking-induced conversion (QuIC) assays leverage protein-amplification and fluorescent signaling for the accurate detection of misfolded proteins. Here, we combine AuNP and QuIC technologies for the visual detection of amplified misfolded prion proteins from tissues of wild white-tailed deer infected with chronic wasting disease (CWD), a prion disease of cervids. Our newly developed assay, MN-QuIC, enables both naked-eye and light-absorbance measurements for detection of misfolded prions. MN-QuIC leverages basic laboratory equipment that is cost-effective and portable, thus facilitating real-time prion diagnostics across a variety of settings. In addition to laboratory-based tests, we deployed to a rural field-station in southeastern Minnesota and tested for CWD on site. We successfully demonstrated that MN-QuIC is functional in a non-traditional laboratory setting by performing a blinded analysis in the field and correctly identifying all CWD positive and CWD not-detected deer at the field site in 24 h, thus documenting the portability of the assay. White-tailed deer tissues used to validate MN-QuIC included medial retropharyngeal lymph nodes, parotid lymph nodes, and palatine tonsils. Importantly, all of the white-tailed deer (n = 63) were independently tested using ELISA, IHC, and/or RT-QuIC technologies and results secured with MN-QuIC were 95.7% and 100% consistent with these tests for positive and non-detected animals, respectively. We hypothesize that electrostatic forces help govern the AuNP/prion interactions and conclude that MN-QuIC has great potential for sensitive, field-deployable diagnostics for CWD, with future potential diagnostic applications for a variety of proteopathies.

A common feature of many neurodegenerative diseases is the presence of misfolded proteins that accumulate within the central nervous system, ultimately contributing to advanced neurodegeneration and death. Misfolded protein diseases (proteopathies) impact a wide variety of mammals, including Creutzfeldt-Jakob disease (CJD), Alzheimer's disease, and Parkinson's disease in humans, bovine spongiform encephalopathy (BSE) in cattle, scrapie in sheep, pituitary pars intermedia dysfunction (PPID) in horses and chronic wasting disease (CWD) in cervids[1–5]. Given well-documented diagnostic limitations surrounding proteopathies in both animals and humans, (i.e., poor sensitivity, limited antibodies for immuno-based assays, etc.), it is imperative to develop improved diagnostic assays[2,6–11]. With respect to prion diseases (a proteopathy subclass caused by infectious proteins), tests that could be deployed in a variety of settings (e.g., hospitals, veterinary clinics, food processing plants, field stations, etc.) would greatly aid the detection of infectious prions thus limiting their spread. It is within this framework that we approach the development of diagnostic tools for CWD of cervids, a model neurodegenerative disorder with urgent needs for portable diagnostic assays that would facilitate rapid detection, thus preventing CWD prions from entering human and animal food-chains.

Similar to CJD in humans, which progresses rapidly and is always fatal, and BSE in cattle, CWD is a prion disease or Transmissible Spongiform Encephalopathy (TSE) that is 100% fatal to infected animals and has no treatments or prevention methods[1,12]. CWD impacts cervids across North America, Scandinavia, and South

[1]Department of Electrical and Computer Engineering, University of Minnesota, Minneapolis, MN 55455, USA. [2]Minnesota Center for Prion Research and Outreach (MNPRO), University of Minnesota, St. Paul, MN 55108, USA. [3]Department of Veterinary and Biomedical Sciences, University of Minnesota, St. Paul, MN 55108, USA. [4]Department of Veterinary Population Medicine, University of Minnesota, St. Paul, MN 55108, USA. ✉email: sang@umn.edu; plarsen@umn.edu

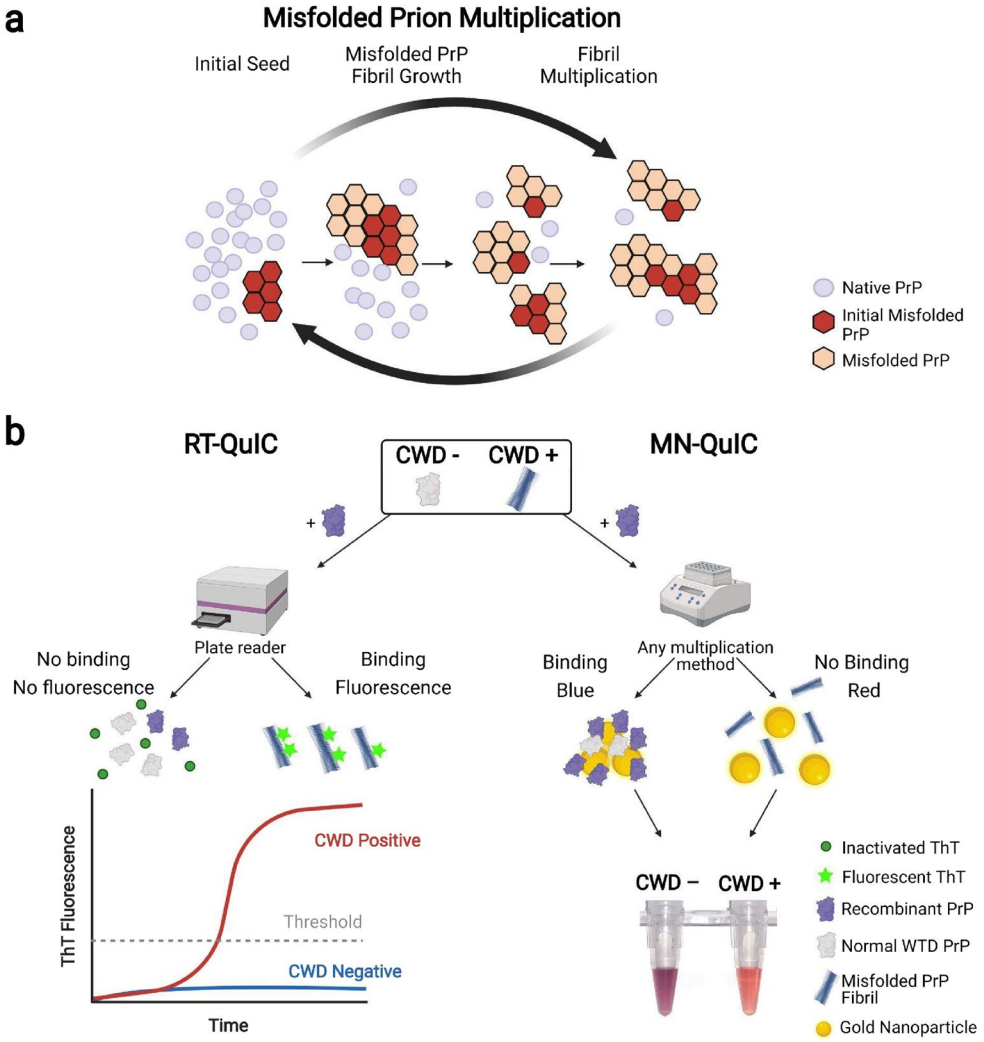

Figure 1. Overview of prion fibril multiplication and two prion amplification assays. (**a**) Schematic of misfolded prion fibril growth. The initial misfolded PrP (PrP^{CWD}) causes native PrP to misfold. (**b**) Overview of RT-QuIC and MN-QuIC. RT-QuIC: Seeds originating from tissue samples of cervids (whether CWD negative or CWD positive) are added to recombinant PrP solutions. These solutions are then shaken and incubated for ~ 48 h (depending on sample type). If present, misfolded PrP fibrils (PrP^{CWD}) from CWD positive tissue induce conformational changes of the recombinant PrP. Amplification results are read in real-time with ThT fluorescence. MN-QuIC: After 24 h amplification, products are diluted and added to an AuNP solution. CWD positive samples result in a red solution (peak absorbance wavelength ~ 516 nm) while CWD negative solutions are blue/purple (peak absorbance wavelength ~ 560 nm).

Korea[13,14] (e.g., elk, moose, mule deer, white-tailed deer, reindeer). The disease continues to spread to new cervid populations, and there are increasing health concerns for both humans and animals exposed to various CWD prion strains[13–15]. All mammals have native functioning cellular prion protein (PrP) distributed throughout various tissues and playing essential roles in a variety of physiological functions, especially those of the central nervous system[16]. Like other protein misfolding neurodegenerative disorders, native prions in cervids adopt conformations of misfolded prions (PrP^{CWD}) (Fig. 1a). PrP^{CWD} propagates throughout an infected animal, forming fibrils that accumulate in lymph and nervous tissues, leading to death years after exposure. CWD poses risks to the health of impacted cervid populations globally, and the disease is an immediate threat to not only cervid health, but also all cervid-related economies. Indeed, cervid hunting and related activities generate tens of billions of USD annually in the United States alone[17]. Across the world, cervids provide a wide array of economically/medicinally[18] important products that are routinely consumed and/or used by humans (i.e., venison meat, antler velvet health supplements, antlers, hides, etc.).

Current diagnostic methods for the detection of protein-misfolding diseases, including CWD and other TSEs, are limited[2,6–11]. Commonly utilized TSE diagnostic assays rely heavily on antibody-based enzyme-linked immunosorbent assay (ELISA) and immunohistochemistry (IHC) technologies that are expensive, time-consuming, and require substantial training and expertise to operate[6]. In addition, a major limitation of ELISA and IHC

Method	Amplification	Time of Amplification	Measurement	Signal Type	Detector	References
MN-QuIC	Thermomixer	24 h	End point	Color change (AuNP)	Naked eye	This work
EP-QuIC	Thermomixer	24–48 h	End point	Fluorescence (ThT)	Fluorometer	[22,23]
RT-QuIC	Plate reader	24–48 h	Continuous real time monitoring	Fluorescence (ThT)	Fluorometer	[6,24–27]

Table 1. Comparison among quaking amplification assays.

assays is that the antibodies routinely used cannot differentiate between native PrP and misfolded TSE-associated prion proteins (PrP^{TSE}) thus requiring protein digestion to enrich for PrP^{TSE}, a methodology that may impact diagnostic sensitivity through the destruction of particular TSE-affiliated PrP strains[19,20]. Collectively, these antibody-based assays are limited in the identification of early-stage TSE infections, and they are primarily used on tissues collected post-mortem.

The detection of prion seeding activity was recently enhanced by various assays involving the amplification of protein misfolding in vitro, including protein misfolding cyclic amplification (PMCA)[6,21], end-point quaking-induced conversion (EP-QuIC)[22,23] and real-time quaking-induced conversion (RT-QuIC)[6,24–27]. Of these prion amplification methods, both EP-QuIC and RT-QuIC (Fig. 1b) utilize a recombinant mammalian PrP substrate (rPrP) that is incubated and shaken with the diagnostic samples. When PrP^{TSE} is present within a given QuIC reaction, it induces a conformational change of the rPrP, forming a beta-sheet enriched mixture that is quantified with fluorescent Thioflavin T (ThT) measurements. Despite the advantages of EP-QuIC and RT-QuIC, there still remain major limitations, including the need for expensive and large laboratory equipment and complex strategies for visualizing and analyzing results, thus limiting access to diagnostic tests. In short, more effective TSE diagnostic methods that leverage small and portable equipment with easily interpretable results are needed to rapidly detect various TSEs in widespread surveillance and prevent additional spread and introduction of TSE prions into human and animal food chains. This is especially true for CWD, as the disease continues to expand across both farmed and wild cervid populations.

In parallel to diagnostic advancements based on prion and protein amplification methods, gold nanoparticles (AuNPs) have been increasingly used for medical applications including disease diagnostics[28–30], drinking water safety[31], and food safety[32]. Due to localized surface plasmon resonances (density fluctuation of conduction electrons)[33], AuNPs have optical absorption peaks that are sensitive to the environment at the AuNP's surface[33–37]. These unique optical properties make plasmonic nanoparticles useful in color-based detection assays[38,39]. Previous studies have indicated affinities of prion proteins with a variety of bare and functionalized metals, including gold[39–42]. One limitation of AuNPs is that they are susceptible to nonspecific binding[43]. Real biological samples are not homogeneous and have many different proteins, ions, and other organic molecules associated with them that can induce AuNPs to spontaneously aggregate making effective AuNP diagnostics challenging. To overcome this, we sought to demonstrate the diagnostic utility of gold nanoparticles for detecting misfolded PrP^{CWD} within QuIC amplified products of CWD positive and negative white-tailed deer (WTD) tissues in homogeneous recombinant hamster prion protein substrates.

By combining the unique plasmonic properties of AuNPs and the methods of quaking-based prion protein fibril amplification, we have successfully overcome the challenges associated with AuNP diagnostics in biological samples and have produced a nanoparticle-based assay (herein named Minnesota-QuIC; MN-QuIC) that can detect the presence or absence of misfolded PrP^{CWD} using both visual and spectroscopic methods (Fig. 1b; Table 1). This method uses only basic lab equipment which reduces assay cost and facilitates deployment outside a traditional laboratory setting. In March of 2021, we deployed the MN-QuIC assay to a field station in rural southeastern Minnesota where the Minnesota Department of Natural Resources (DNR) was performing its annual CWD surveillance and targeted culling efforts. We demonstrated proof-of-concept experiments for MN-QuIC's utility as a portable prion assay by successfully detecting CWD-infected WTD tissues at the DNR field station.

Results

Gold nanoparticle interaction with native cellular prions vs. misfolded fibrils. To investigate whether AuNPs can differentiate between misfolded PrP fibrils and native PrP originating from recombinant hamster prion protein (rPrP), two sets of reaction mixtures seeded with and without spontaneously misfolded rPrP prion fibrils were processed following modified RT-QuIC protocols without ThT[44,45]. The presence of fibril formation was examined in all reaction mixtures by adding and quantifying ThT post hoc (Fig. S1a). ThT fluorescence was significantly different between misfolded rPrP (seeded) and native non-misfolded rPrP (no seed) ($p = 0.05$; Fig. S1a). We hypothesized that misfolded prion fibrils would interact differently with AuNPs, as compared with native rPrP, and that the interaction would influence AuNP aggregation as measured by dynamic light scattering (DLS). Following ThT quantification, misfolded rPrP samples and native rPrP samples were spiked into separate AuNP solutions. After a 30 min incubation period at ambient temperature, there was a visible color difference between the AuNP solutions spiked with misfolded and native rPrP similar to the change in Fig. 1b. This was also reflected in the visible spectrum of the absorbance peak (Fig. 2a).

Color changes due to AuNP aggregation have been reported in the literature for a variety of nanoparticle/protein combinations[38,39]. DLS experiments were performed on three AuNP solutions (seeded, non-seeded, and blank; see Methods), and average effective particle size was determined for each sample (Fig. 2b). We observed a significant difference of AuNP effective particle sizes between AuNP solutions seeded with misfolded rPrP

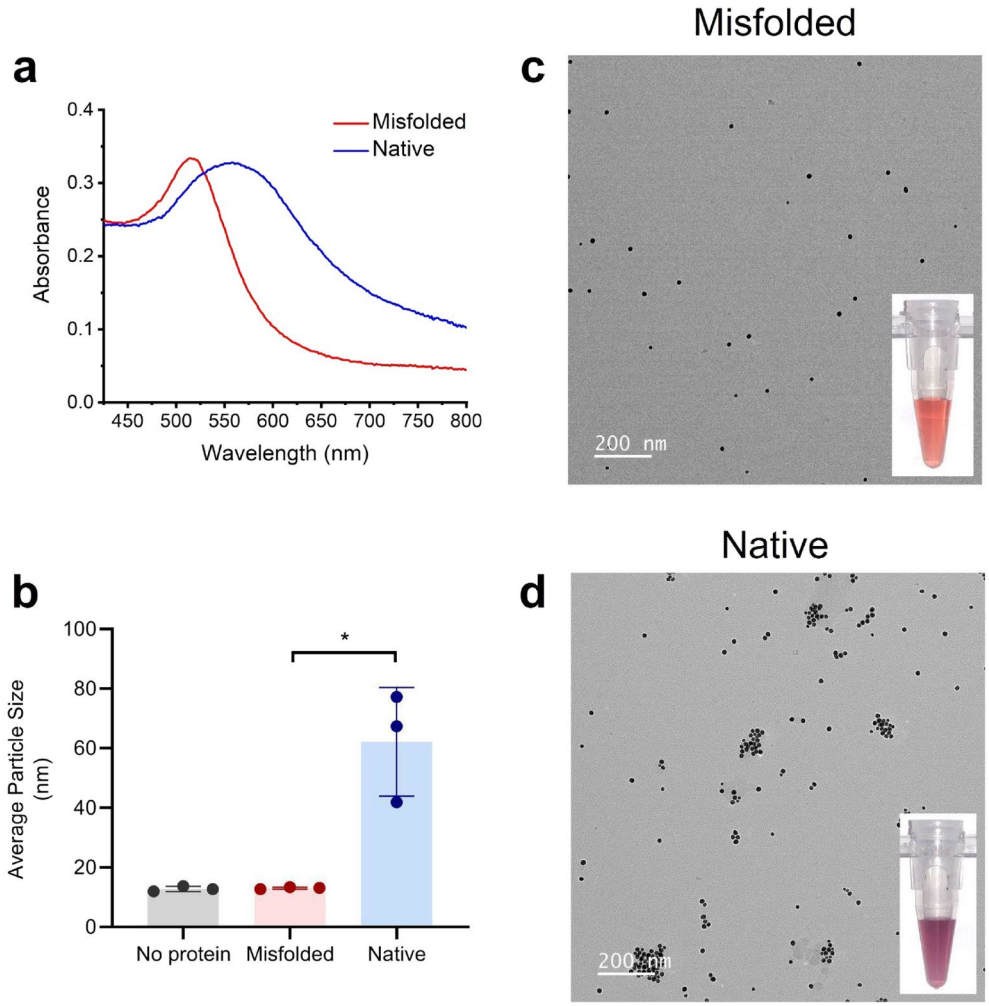

Figure 2. Mechanism of AuNP solution color shift. (**a**) The absorbance spectrum of AuNP solutions spiked with misfolded rPrP from seeded QuIC reactions (red line) and native (non-misfolded) rPrP from QuIC reactions without seed (blue line). (**b**) Average effective particle sizes in AuNP solutions containing no protein, misfolded rPrP, and native rPrP observed by DLS. (**c**) TEM image of 15 nm AuNPs after being spiked with post amplified misfolded PrP. Inset shows an example of AuNP solution after being spiked with misfolded PrP. (**d**) TEM image of aggregating AuNPs after being spiked with native PrP. Inset shows an example of AuNP solution after being spiked with post amplified native PrP. *, p-value < 0.05, error bars show standard deviation.

versus native non-seeded rPrP ($p = 0.05$) (Fig. 2b). The AuNPs spiked with no protein (blank) and misfolded rPrP exhibited similar particle size distributions (Fig. S1b,c), indicating that the misfolded rPrP solutions did not induce AuNP aggregation. On the contrary, the addition of diluted native rPrP resulted in larger particle sizes for AuNPs (Fig. S1d) than AuNPs with no protein added (Fig. S1b), indicating that the addition of diluted native rPrP caused AuNPs to aggregate. To further examine this, AuNP solutions spiked with spontaneously misfolded rPrP and native rPrP were studied in a transmission electron microscope (TEM). Through TEM, it was clear that the AuNPs did not aggregate when spiked with misfolded prion (Fig. 2c). Conversely, it could be seen that AuNPs aggregate in the presence of native rPrP (Fig. 2d). These results were consistent with DLS measurements and indicate differential AuNP binding interaction between native rPrP and misfolded rPrP fibrils.

CWD positive and negative samples produce unique AuNP optical signatures. Understanding that misfolded prions can induce rPrP misfolding and subsequent amplification[46], thus influencing AuNP aggregation (see above), we then investigated the potential of MN-QuIC for CWD diagnostics using PrP^{CWD} positive and negative WTD lymphoid tissues. We used homogenates of independently confirmed CWD positive and negative WTD medial retropharyngeal lymph nodes (RPLN) (Table S1). Independent RT-QuIC analyses were performed on all tissues used for AuNP analyses (Fig. 3a)[27].

In light of our previous results, we anticipated that AuNPs could be utilized to facilitate direct visualization of QuIC-amplified misfolded rPrP solutions that were seeded with CWD positive tissue using a standard benchtop thermomixer. Because thermomixers are more cost effective and have a smaller footprint than plate readers, they have been used previously in conjunction with end-point ThT readings (i.e., EP-QuIC) to determine the

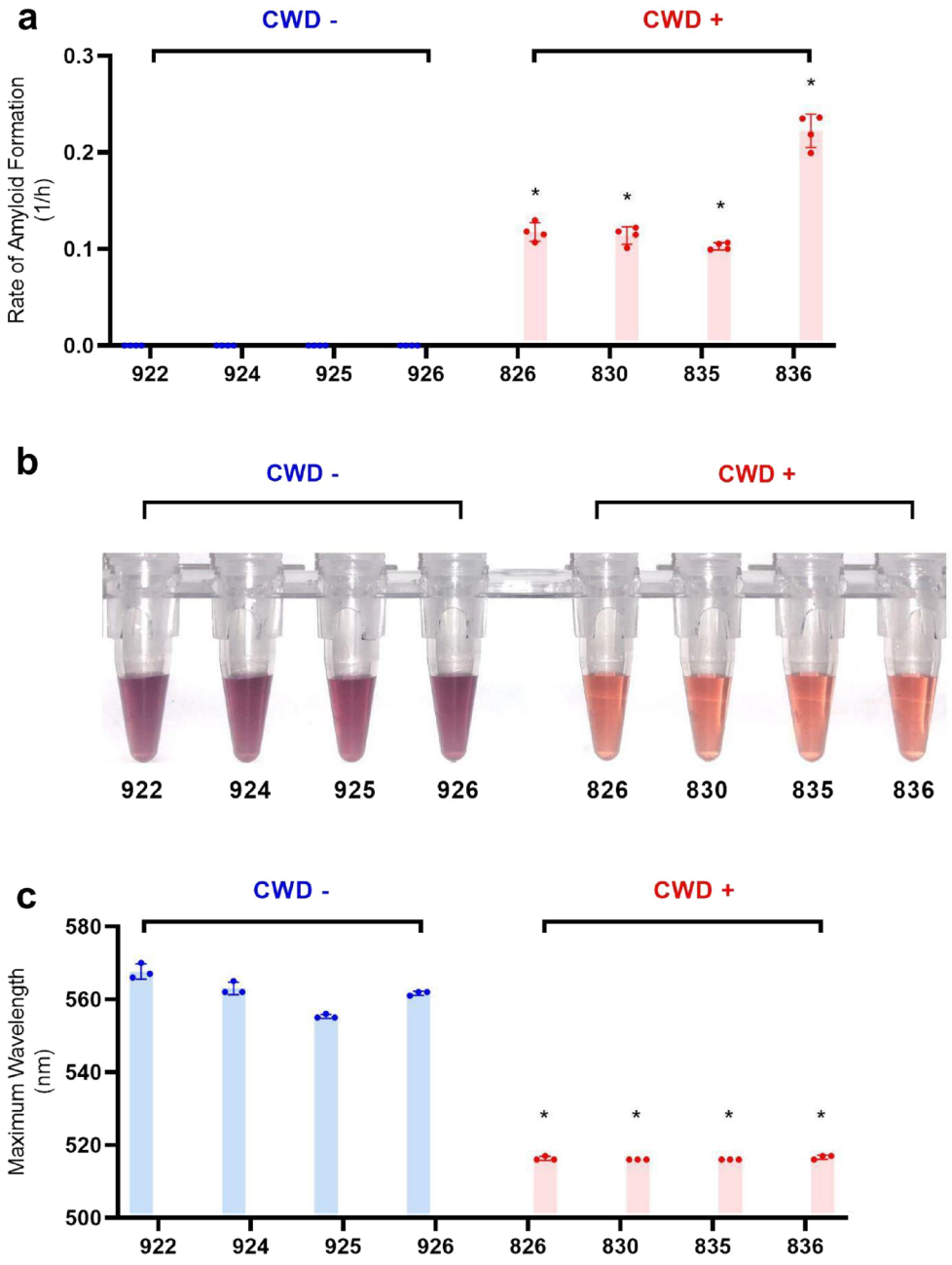

Figure 3. Comparison of RT-QuIC and MN-QuIC results for CWD positive and negative RPLN tissues. MNPRO sample identification number on the horizontal axis. (**a**) RT-QuIC data for the rate of amyloid formation for negative and positive RPLN tissue samples from wild WTD using ThT fluorescence. (**b**) Photo of MN-QuIC tubes showing the color difference for the same set of tissue samples used in (**a**). (**c**) MN-QuIC peak absorbance wavelength of the same set of solutions used in (**b**). *p-value < 0.05, error bars show standard deviation.

presence of CJD prion seeding activity[22,23]. To test this, homogenates from the same set of samples tested with RT-QuIC (Fig. 3a.) were added to the RT-QuIC master mix without ThT on 96-well plates, which were then subjected to shaking/incubation cycles on a thermomixer for 24 h. The post-amplification solutions were then diluted to 50% in buffer and added to AuNP solutions. We found that we were able to clearly distinguish CWD positive and negative samples simply through color difference appreciable by naked eye; the QuIC-amplified CWD positive and negative samples were red and purple, respectively (Fig. 3b).

To quantify our observations and measure statistical differences, the absorbance spectrum of the AuNPs was measured from 400 to 800 nm using a 96-well plate reader. In the resulting absorbance spectrum, AuNP solutions combined with QuIC-amplified CWD positive samples had absorbance peaks near 516 nm (Fig. 3c), similar to the 515 nm absorbance peak of the AuNPs prior to the addition of protein solutions. However, the negative

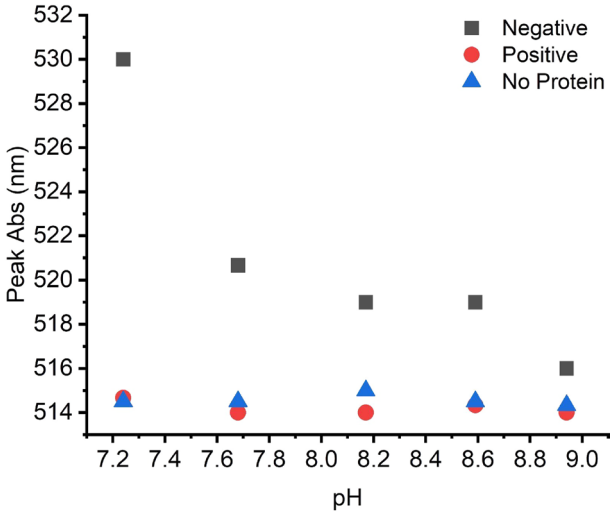

Figure 4. Wavelength of peak absorbance of AuNPs in varying pH buffers containing CWD negative rPrP (square), CWD positive (PrP^{CWD}) (circle), and blank/no protein (triangle) solutions.

sample absorbance peaks were shifted to longer wavelengths of approximately 560 nm (Fig. 3c), confirming that the purple color of AuNP solutions from QuIC products originating from CWD negative tissue samples was consistent with the observed purple color of AuNP aggregates associated with native rPrP (Fig. 2b and Fig S1d). Accordingly, the peak AuNP absorbance wavelengths of CWD negative samples are significantly larger ($p < 0.05$) than CWD-positive samples (Fig. 3c).

Electrostatic forces and rPrP concentration play a role in AuNP-based CWD detection. Considering the results described above, we aimed to determine the mechanism underlying AuNP aggregation caused by native rPrP solutions. Studies of prions and other proteins have shown that electrostatic forces help govern the interactions between nanoparticles and proteins[39,47,48]. Because the theoretical isoelectric point (pI) of our rPrP is around pH 8.9[49], rPrP is positively charged in the pH 7.4 AuNP buffer whereas citrate capped AuNPs are negatively charged even at pHs well below our buffer[50]. Thus at pH 7.4, there exists an electrostatic attractive force between AuNPs and native rPrP that contributes to their interactions (AuNP aggregation and the color change). The charge on the protein changes when the pH of the environment is altered and thus the interaction between AuNP and rPrP is disrupted. When the pH of a solution is raised closer to the IP of the rPrP, the charge of the protein will become closer to neutral, decreasing the force of attraction between AuNP and rPrP. We showed that as the pH of the AuNP solution was raised closer to the IP of native rPrP, the absorbance peak of the AuNP-rPrP solution decreased from 530 nm (Fig. 4) while the control AuNP solution with no protein had very little peak deviation from 515 nm. This indicates that electrostatic interactions were partially responsible for facilitating the native rPrP interactions with AuNPs. QuIC-amplified PrP^{CWD} products, on the other hand, have experienced major conformational changes from their native form (as confirmed by ThT beta-sheet binding; Fig. 3a) and have formed fibrils. These fibrils can further clump to form large tangled structures, reducing the effective concentration of rPrP in the reaction. When there is a low concentration of free-floating rPrP in the solution, the interaction between prions and AuNPs drops below detectable levels (Fig. S2). Because of the concentration effects from large fibril formation, the interaction between positive (misfolded) prions and AuNPs is unaltered by pH (Fig. 4).

Field deployment and high-throughput protocols. To show the potential for a portable, field-deployable diagnostic, we performed proof-of-concept experiments at a rural Minnesota DNR field station (Fig. 5a). We tested both pooled and individual tissues consisting of medial retropharyngeal lymph nodes, parotid lymph nodes, and palatine tonsils tissues from 13 WTD that the DNR had recently collected from the surrounding wild deer population. Three of these animals (blinded to the field team) were CWD positive as determined by regulatory ELISA and IHC testing of medial retropharyngeal lymph nodes. Using a blinded testing approach, MN-QuIC successfully detected all three CWD positive animals via visibly red AuNP solutions (Fig. 5b). We obtained CWD not detected or negative results (purple AuNP solutions) for the 10 animals that were independently identified by ELISA as CWD not detected (Table S2). These proof-of-concept experiments demonstrate the potential utility of MN-QuIC as a portable, field-deployable diagnostic tool for researchers and agencies.

Through field deployment, we conceived and developed a high-throughput protocol for MN-QuIC. In order to examine its reliability, a blinded set of an additional 20 CWD negative and 20 CWD positive WTD RPLNs (Table S3) were tested in a 96-well format in the laboratory. The CWD status of these tissues was independently confirmed by ELISA and/or IHC. For MN-QuIC, each sample had eight replicates and was prepared and subjected to the QuIC protocol using a 96-well plate on a thermomixer for 24 h. A multichannel pipette was then used to add the QuIC amplified protein to a separate 96-well plate filled with AuNP solution and subsequent

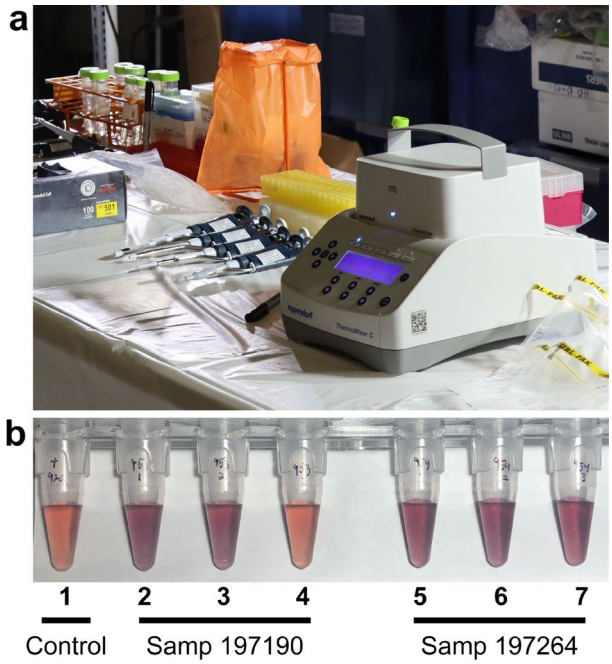

Figure 5. Images from experiments performed in the field. (**a**) Portable MN-QuIC setup used during field deployment. (**b**) Example of observed visible color of the MN-QuIC reaction when testing for CWD. Far-left tube (Tube 1) is a positive control, followed by CWD not-detected tube (in purple; Tubes 2, 3, 5, 6, 7) and a single CWD positive tube (in red; Tube 4). Tubes 2–4 correspond to animal 197190 in Table S2 and tubes 5–7 correspond to animal 197264 in Table S2.

color changes were observed within the first minute. For RT-QuIC analyses, it is common practice to consider a particular sample positive if 50% or more of its wells are positive[24,51–53]. Using this approach, we successfully identified 18 out of 20 CWD positive tissues and 20 out of 20 CWD negative tissues in the blinded sample set using MN-QuIC (Table S3).

To show MN-QuIC's versatility with other tissue types, palatine tonsils from a set of 10 CWD negative and 10 CWD positive WTD (Table S4) were tested using the same protocol used for the blinded set of 40 RPLNs (eight AuNP replicates in a 96-well plate). The CWD status of the palatine tonsil tissues was independently confirmed with RT-QuIC (Fig. 6a). CWD positive samples were identified using a threshold of 50% or more of wells being red (i.e., majority red in color), and we correctly identified 100% of CWD positive samples with no false positives using the MN-QuIC assay (Fig. 6b; Tables S4, S5). In addition to visual color, these results were assessed by investigating the peak shift from the expected 517 nm (red) for positive samples and all red wells had absorbance peaks within 4 nm of 517 nm.

Sensitivity, specificity and serial dilutions. Table S5 reports the sensitivity and specificity for each individual sample set tested herein. Overall sensitivity and specificity of MN-QuIC compared to RPLN ELISA/IHC, when combining all animals from the sample sets presented in Tables S1-S4, was found to be 95.7% (95% confidence interval = 79–99%) and 100% (95% confidence interval = 91–100%), respectively. To examine the lower limit of CWD detection for MN-QuIC, two 96-well plates with serial dilutions (8 replicates each) of a CWD positive parotid lymph node ranging from 10^{-1} to 10^{-8} were created and shaken/incubated for 24 h on a thermomixer (MN-QuIC) and plate reader (RT-QuIC), respectively. Within 24 h both MN-QuIC and RT-QuIC detected seeding for replicate(s) from 10^{-2} to 10^{-6} (Table 2). Interestingly, RT-QuIC was unable to detect PrP^{CWD} seeding activity at a 10^{-1} dilution (eight replicates with no amyloid formation), perhaps due to a higher concentration of inhibitors (vs. 10^{-2}, etc.). However, four of eight replicates for the 10^{-1} dilution were positive using MN-QuIC.

Discussion

Given the continued spread of CWD among cervid populations throughout North America, Northern Europe, and South Korea[13,14] there is an urgent need to develop widely accessible diagnostic tools for CWD. Historically, AuNP colorimetric assays have been limited because of spontaneous AuNP aggregation issues when used with biological samples[43]. Here, we combined QuIC amplification of CWD prions with the simplicity of gold nanoparticles to effectively eliminate spontaneous AuNP aggregation challenges and to enable the visualization of positive vs. negative CWD lymph node and palatine tonsil WTD samples. We hypothesized that the conformational differences between the native rPrP substrate and misfolded prion fibrils would influence the aggregation of AuNPs in solution.

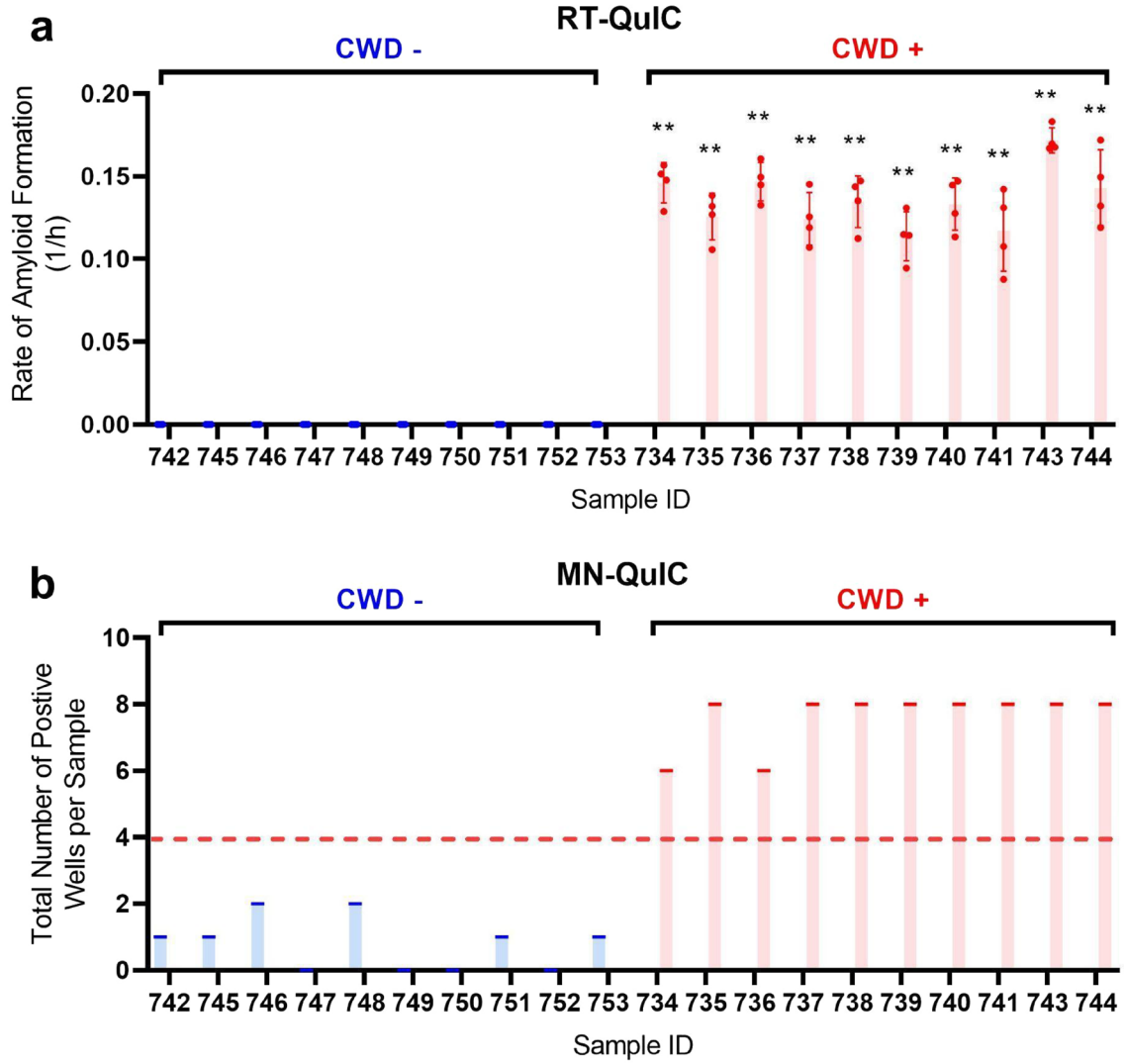

Figure 6. Comparison of RT-QuIC and MN-QuIC results for CWD positive and negative palatine tonsil tissues. MNPRO sample process identification number on horizontal axes (**a**). Fluorescent RT-QuIC data for tissues (see Supplementary Table S4) used in (**b**). (**b**) MN-QuIC data for tonsil samples used in this study. Number of red wells out of the 8 replicates for each sample tested. Following published RT-QuIC protocols (see Results and discussion) 50% or more of MN-QuIC red wells are identified as CWD positive and less than 50% of MN-QuIC red wells as CWD not detected or negative. $^{**}p < 0.01$, error bars show standard deviation.

Dilution Factor	Number of Replicates with Seeding Detected via MN-QuIC	Number of Replicates with Seeding Detected via RT-QuIC
10^{-1}	4	0
10^{-2}	8	8
10^{-3}	8	8
10^{-4}	8	8
10^{-5}	4	8
10^{-6}	1	8
10^{-7}	0	0
10^{-8}	0	0

Table 2. Serial dilution: Dilutions of CWD positive parotid lymph node run for 24 h via MN-QuIC vs 24 h via RT-QuIC.

By injecting post-QuIC-amplified protein solutions into AuNPs, we were able to clearly distinguish (via visible color change) between CWD positive and CWD negative medial retropharyngeal lymph node and palatine tonsil tissues. AuNP solutions for these positive and negative samples appeared red and purple, respectively. We further confirmed that the color change was a result of the aggregation of AuNPs by conducting DLS and TEM experiments that compared the effective particle sizes in the presence of native and misfolded rPrP. We observed that the AuNP aggregation was governed by electrostatic interactions by altering the pH of the solution. Finally, we demonstrated proof-of-concept experiments for the practical utility of MN-QuIC by successfully identifying CWD-infected WTD tissues at a DNR field station in southeastern MN.

We estimated the sensitivity and specificity of MN-QuIC for CWD detection (across several tissue types from individual WTD) in comparison to diagnosis by ELISA/IHC using RPLNs, the standard of practice for CWD diagnosis in WTD (Table S5)[27]. It is important to note that where tissue types differ, we are not only comparing diagnostic test performance, but also the probability that a certain tissue type will contain detectable levels of PrP^{CWD} as compared to RPLN. Yet, tissue distribution of PrP^{CWD} can vary based on route of infection, stage of infection, and prion strain[54–56]. We also recognize that under conditions of natural infection, the assumption that ELISA and IHC are a "gold standard" for diagnostic test comparison may be inappropriate given that these tests are imperfect[57]. Knowing these limitations, estimates of diagnostic test performance warrant further evaluation using methods that can overcome the constraints related to reliance on a "gold standard" comparison[57–60].

Dilution experiments comparing MN-QuIC and RT-QuIC after 24 h reveal that both MN-QuIC and RT-QuIC can detect signs of PrP^{CWD} seeding activity down to 10^{-6} homogenate solutions (Table 2). It should be noted that RT-QuIC had more replicates detect seeding at low dilutions than MN-QuIC. However, this could be due to the exclusion of N-2 supplement from MN-QuIC homogenate dilutions in this study due to concerns that it may affect prion–AuNP interaction. N-2 coats the walls of RT-QuIC dilution tubes which aids the detection of extremely low prion content. The observation that both methods detected PrP^{CWD} seeding down to 10^{-6} dilutions is significant because it suggests that MN-QuIC has similar sensitivity to RT-QuIC.

Of all samples tested, there were only two CWD positive RPLNs (sample process IDs 923 and 926) where MN-QuIC was not consistent with ELISA or RT-QuIC results (Table S3). For these samples, two of eight replicates turned red and thus using the 50% red well threshold were classified as PrP^{CWD} not-detected via MN-QuIC in contrast to a CWD positive classification from ELISA and RT-QuIC testing. However it should be noted that when independently tested, the RPLN from sample 923 exhibited low ELISA optical density (OD) and a low rate of amyloid formation on RT-QuIC, likely indicating relatively low levels of PrP^{CWD} within the tissue. Using MN-QuIC, sample 926 (animal ID 832) was found to be negative on RPLN (Table S3), however MN-QuIC identified this same animal (animal ID 832) as positive on palatine tonsils (Table S4). Tissue sampling variability, particularly with low levels of PrP^{CWD}, can affect test outcome when using uni-lateral sampling (i.e., testing only the left RPLN) or different subsamples from the same tissue[61].

The primary laboratory equipment for MN-QuIC consists of a tissue homogenizer, temperature-controlled shaker, and if desired (but not necessary), a spectrometer for light absorbance readings in addition to visual observations. Compared to EP-QuIC/RT-QuIC and PMCA, which leverage ThT fluorescence and antibody-based Western blotting, respectively[6], results from MN-QuIC can be visualized with the naked eye or quantified using simply light-absorbance readings. Because MN-QuIC is a protein amplification method, it can be adapted to examine any tissue or biological sample that existing and future RT-QuIC protocols use, thus giving MN-QuIC wide versatility. Studies have shown that amplification-based assays, such as RT-QuIC, are more sensitive than conventional ELISA[62]. Given that MN-QuIC has similar sensitivity to RT-QuIC (Table 2) and uses a similar amplification method, MN-QuIC has the potential to have increased sensitivity compared to ELISA. Recent publications have used specially functionalized AuNPs to detect a variety of protein targets[39,63–65]. However, the AuNPs used here are capped with citrate, which is one of the most common methods for stabilization making it simple and widely commercially available. For this reason, MN-QuIC offers a cost-effective approach to CWD testing as less than $1.00 USD of AuNPs are used per sample (including 8 replicates). When including reagent and production costs for recombinant hamster protein, the approximate MN-QuIC cost per sample is nearly the same as RT-QuIC (~ $12.00 to $15.00 USD per sample; four to eight replicates). At the time of publication, the cost of equipment for MN-QuIC is just 20% (~ $6000 USD) of that which is needed for RT-QuIC (~ $30,000 USD) and slightly over 50% of that used in low-throughput ELISA (~ $11,000 USD). By eliminating the need for time consuming preparation and/or the relatively expensive visualization strategies used in EP-QuIC, RT-QuIC, ELISA, IHC and/or PMCA, MN-QuIC provides new opportunities for widely accessible and sensitive CWD diagnostics.

AuNPs have been used in a variety of advanced sensing applications[28,29,31–33,66,67]. Our work demonstrates that AuNPs can open promising avenues for the identification of misfolded prions. Because prion proteins have strong interactions with simply functionalized metallic surfaces, besides AuNPs, we envision a broad range of metallic nanoparticles with various materials and shapes to be useful in detection. Additionally, substrate-based nanostructures exhibiting optical resonances could be useful in detecting conformational changes via other sensing modalities such as surface-enhanced infrared absorption spectroscopy[68,69] to further improve the speed and accuracy of prion detection. Examining other areas of the electromagnetic spectrum, such as tera-Hertz sensing, could also lead to improved detection[70].

To demonstrate field deployment capabilities of the MN-QuIC assay, we collected medial retropharyngeal lymph nodes, parotid lymph nodes, and palatine tonsil samples from 13 WTD at a rural DNR field station. Using both pooled and individual tissues of these 13 individuals, MN-QuIC was 100% successful in identifying three CWD positive and 10 CWD not-detected animals. The successful field-based classification of these animals provides clear proof-of-concept demonstration of MN-QuIC's utility as a portable and sensitive field test. We note that our MN-QuIC analysis has a low false-negative rate, and has yet to produce a statistically significant false positive result. These observations are critically important when considering MN-QuIC as a field-based

diagnostic tool for CWD. Moreover, any positive result can be independently validated using downstream RT-QuIC, ELISA, and/or IHC testing. Given growing concerns of CWD prion strain variation and risks to human and animal health[15], any field-based diagnostic assay that avoids producing false-negative is preferred.

RPLN and palatine tonsils collected from WTD were the basis for the laboratory-based analyses conducted herein because these tissues are ideal for early and accurate identification of CWD infection, with tonsils additionally having antemortem applications[27,71]. Future studies should be performed using MN-QuIC on large sample sets to better characterize MN-QuIC's sensitivity and specificity for specific tissues. Additional work will focus on leveraging MN-QuIC for CWD diagnostics using a variety of antemortem biological samples (e.g., blood, saliva, and feces). RT-QuIC amplification assays using samples acquired from living deer have recently been reported[45,72] and these assays could be readily combined with MN-QuIC to provide field-deployable antemortem tests of both wild and farmed cervids. Moreover, MN-QuIC may have potential food-safety test applications given the recent documentation of RT-QuIC-based detection of CWD prions in WTD muscles used for human and animal consumption[26].

The mechanisms underlying interactions between AuNPs and various prion proteins are underexplored, given the results reported herein a detailed characterization of AuNP–prion interactions is highly desirable. Based on the available knowledge in the field, we hypothesized that as the pH approaches the prion's isoelectric point, the electrostatic force of attraction between the negatively charged citrate capped AuNP and the protein would decrease. Our analyses revealed that as the pH neared the theoretical isoelectric point of rPrP, the wavelength of the peak absorbance of the AuNPs spiked with native (CWD negative) protein decreased. We also found that pH alterations had little effect on AuNP solutions without protein, indicating that the effect of pH on native rPrP-spiked AuNP solutions was not caused by intrinsic AuNP aggregation in response to the changing pH. QuIC-amplified CWD positive solutions did not change with varying pH because of fibril formation effects on free-floating prion concentration. Therefore, the difference in interactions between CWD negative and positive solutions is likely governed by electrostatic forces and rPrP concentration effects. However, other factors such as hydrophobic interactions[73,74] could also play a role. Various studies have shown that both native and misfolded PrP bind various metal ions and bulk metals including gold[16,40–42]. Our research reveals AuNPs stabilized with a simple citrate capping readily interact with the truncated rPrP substrate that is used as the primary substrate for a growing variety of QuIC assays. Future structural analyses focused on native rPrP and prion fibrils[75] could provide further insight into how native rPrP, but not misfolded rPrP fibrils, influence AuNP aggregation.

Conclusions

MN-QuIC holds great promise not only for the visual detection of CWD-positive samples but also for the detection of other protein misfolding diseases. The need for inexpensive, sensitive, widely deployable diagnostics for neurodegenerative diseases is only growing as neurodegenerative diseases are predicted to greatly increase in the next decades[2,76]. It has been proposed that advances in CWD diagnostics will yield technologies that are useful for a broad range of neurodegenerative diseases[6]. RT-QuIC protocols have already been developed for a number of sample types allowing for antemortem tests[45,72]. These and future amplification methods could readily be combined with MN-QuIC. Additionally, QuIC amplification protocols have been developed for a variety of other protein misfolding diseases including scrapie in sheep[77], BSE in cattle[78], and Alzheimer's[79], Parkinson's[52,80], and CJD in humans[22,23]. Thus, we posit that the combination of AuNP technology with protein amplification assays has great potential for the development of versatile neurodegenerative disease diagnostic platforms. By eliminating the need for expensive/complicated visualization schemes, our hybrid assay technology has the potential to greatly increase access to neurodegenerative disease diagnostics. It is our vision that in the future, variations of this AuNP-based protein amplification/detection assay could be deployed in medical clinics around the world to aid in neurodegenerative diagnosis and early application of therapeutics.

Methods

Tissue preparation. 60 WTD tissues (30 CWD-negative and 30 CWD-positive; from 50 animals) were selected for laboratory-based RT-QuIC and MN-QuIC analyses (Tables S1, S3, S4 and S5). These samples were collected from WTD through collaboration with the Minnesota DNR (Schwabenlander et al.[27]; Tables S1, S3 and S4), and their CWD status was independently identified utilizing the Bio-Rad TeSeE Short Assay Protocol (SAP) Combo Kit (BioRad Laboratories Inc., Hercules, CA, USA). Positive RPLNs were confirmed by IHC at the Colorado State University Veterinary Diagnostic Laboratory. Metadata containing information of all specimens examined in the lab, including tissue type, is provided in supplementary materials (Tables S1, S3 and S4). Supporting Table S5 provides a summary of the MN-QuIC results used in this study and their classification compared to independent testing. WTD RPLNs (Tables S1 and S3) and palatine tonsils (Table S4) were homogenized in PBS (10% w:v) in 2 mL tubes containing 1.5 mm zirconium beads with a BeadBug Homogenizer (Benchmark Scientific, Sayreville New Jersey, USA) on max speed for 90 s. These samples are referred to as 10% homogenates. All CWD positive and negative samples were selected based on independent ELISA, IHC, and/or RT-QuIC results and were subsampled using methods as reported in Schwabenlander et al.[27].

Preparation of recombinant substrate. Recombinant hamster PrP (HaPrP90-231) production and purification followed the methods in Schwabenlander et al.[27] The substrate is derived from a truncated form (amino acids 90–231) of the Syrian hamster PRNP gene cloned into the pET41-a(+) expression vector and was expressed in Rosetta (DE3) *E. coli*. The original clone was provided by the National Institutes of Health Rocky Mountain Laboratory. Many studies have utilized haPrP for RT-QuIC[7,26,27,44,45]. Recombinant hamster PrP was used in this study due to its seemingly universal proclivity to misfold in the presence of infectious prions for a large variety of species.

QuIC for lymph tissues. For QuIC analysis (both MN-QuIC and RT-QuIC), a master mix was made to the following specifications: 1X PBS, 1 mM Ethylenediaminetetraacetic acid (EDTA), 170 mM NaCl, 10 µM thioflavin T (ThT), and 0.1 mg/mL rPrP. In instances where the end reaction would be analyzed using AuNPs, ThT could be excluded. The 10% tissue homogenates (prepared as described above) were further diluted 100-fold in 0.1% Sodium Dodecyl Sulfate (SDS) using methods from Schwabenlander et al.[27] (final tissue dilution: 0.1%). 1ul of N-2 Supplement [Life Technologies Corporation, Carlsbad, California, USA]) was added to 99ul dilution of SDS (for MN-QuIC reactions N-2 was excluded from SDS). 2 µL of the diluent were added to each well containing 98 uL of master mix. Plates for RT-QuIC were amplified on a FLUOstar® Omega plate reader (BMG Labtech, Cary, North Carolina, USA; 42 °C, 700 rpm, double orbital, shake for 57 s, rest for 83 s). Fluorescent readings were taken at ~ 45 min increments.

Thermomixer-based amplification. For MN-QuIC, we leveraged a standard benchtop shaking incubator (thermomixer) to produce QuIC-based prion amplifications as previously reported by Cheng et al.[22] and Vendramelli et al.[23], although with slight modifications. Plates were prepared identically to those amplified on the plate reader (see protocol above). Instead of shaking on a plate reader, reactions were performed on a ThermoMixer® C equipped with SmartBlock plate and Thermotop (Eppendorf, Enfield, Connecticut, USA) at 48 °C for 24 h at 600 RPM (60 s shake and 60 s rest). We selected a 24 h run time based on independent RT-QuIC results for RPLNs and palatine tonsils from CWD positive WTD reported in Schwabenlander et al.[27], including those examined herein, showing significant seeding activity within 9 to 24 h (Fig. S3). The resultant products were visualized with the addition of gold nanoparticles (as described below).

Spontaneous misfolding of rPrP for DLS Experiment. Spontaneous misfolding of recombinant prion protein was generated similarly standard RT-QuIC but with unfiltered recombinant proteins and reagents. For these reactions, no infectious seed was necessary. The spontaneously misfolded material was used to seed reactions for the dynamic light scattering experiment, described below.

Preparation of gold nanoparticles. Post-amplified material was visualized with 15 nm citrate-capped gold nanoparticles purchased from Nanopartz (Loveland, Colorado, USA) with stock concentrations ranging from 2.45 nM to 2.7 nM. AuNP protocols were modified from Špringer et al.[81] and Zhang et al.[39] AuNPs were buffer exchanged using 530ul of stock solution that was centrifuged in 1.6 mL tubes at 13,800 g for 10 min. 490ul of supernatant was removed and the undisturbed pellet was resuspended with 320ul of a low concentration phosphate buffer (PBS_{low}; pH 7.4 via addition of HCl) made of 10 mM Na_2HPO_4(Anhydrous), 2.7 mM KCl, 1.8 mM KH_2PO_4). After the quaking/incubation steps, protein solutions were diluted to 50% in MN-QuIC buffer (pH 7.2), consisting of 1X PBS with the addition of final concentrations of 1 mM EDTA, 170 mM NaCl, 1.266 mM sodium phosphate. Forty microliters of the protein diluted 50% in MN-QuIC buffer were then added to the 360ul AuNP solution with ample mixing (results shown in Fig. 3b,c). This solution was left to react at room temperature (RT) for 30 min (although a visible color change is observable within 60 s) before visual color was recorded (purple or red) and photographed. After images were taken, three replicates of 100ul were taken from the 400ul AuNP mixture and pipetted into three separate wells of a 96-well plate. The absorbance spectrum was then recorded for each well at wavelengths 400–800 nm using the FLUOstar® Omega plate reader (BMG Labtech, Cary, North Carolina, USA).

For AuNP visualization experiments performed to determine higher throughput capacity (Fig. 6; Tables S3, S4), proteins were prepared in the same way. After amplification on the thermomixer, proteins on a 96-well plate were diluted to 50% using MN-QuIC buffer and a multichannel pipette. 90ul of AuNPs were then added to a separate non-binding 96-well plate. The AuNP wells were spiked with 10ul of the diluted protein from the thermomixer (post-amplification) using a multichannel pipette. After waiting 30 min, the color changes were observed and the absorbance spectrum of the plate was taken.

Dynamic light scattering. Spontaneously misfolded rPrP samples (described above) were produced from solutions of rPrP with no seed added. In addition to these samples, a 96-well RT-QuIC reaction was performed with half the wells consisting of native rPrP seeded with spontaneously misfolded rPrP, and half consisting of native rPrP with no seed. The 96-well plate was then amplified using QuIC protocols described above. Post-amplification, seeded samples were confirmed to have fibrillation while the non-seeded samples were confirmed to not have fibrillation based on ThT binding (described above). Seeded and non-seeded samples were diluted to 50% in MN-QuIC buffer, and 40ul of these solutions were added to 360ul of AuNPs in PBS_{low}. Additionally, a blank with no protein was produced by adding 40ul of MN-QuIC buffer to 360ul of AuNPs in PBS_{low}. For native rPrP samples, color change was observed within 1 min of rPrP addition. No color change was observed in spontaneously misfolded rPrP samples at any time length. Dynamic light scattering measurements of all samples were taken after 5 min of protein addition using a Microtract NanoFlex Dynamic Light Scattering Particle Analyzer (Verder Scientific, Montgomeryville, PA, USA), and measurement times were 60 s. Five measurements were taken for each sample and then averaged.

TEM measurements. TEM measurements were performed using a Tecnai G2 F30 Transmission Electron Microscope. Images were recorded on a Gatan K2 Summit direct electron detector. 20ul of post-amplified positive and negative rPrP were added to separate volumes of 200ul of AuNPs prepared as described above. Each protein solution was added to separate uncharged TEM grids. Stain was not used because it was unnecessary to view the AuNPs.

Effects of pH and rPrP substrate concentration on the AuNP-protein interaction. In order to test the effects of pH on the interaction of rPrP with AuNP, five different 10 mM tris-buffer solutions with pHs ranging from 7.2 to 9.0 were created. Tris was used to give buffering for the desired pH range. AuNPs were buffer exchanged as described above except tris-buffer was used instead of PBS_{low}. Protein solutions were added as previously described. It can be noted that the peak absorbance for the tris buffer solution below pH 7.4 is still not as high as the peak shifts in pH 7.4 PBS_{low}. This is likely due to the differences in tris and PBS_{low} buffers.

To examine effects of rPrP substrate concentration (Fig. S2), six different master mixes were made with concentrations of native rPrP ranging from 0 mg/ml to 0.1 mg/ml. 10ul of each solution were added to separate wells containing 90ul AuNPs (pH 7.4 AuNPs prepared as described above).

Additional statistical information. We estimated Wilson Score confidence intervals for MN-QuIC sensitivity and specificity estimates in Epitools[82]. Wilson confidence intervals are appropriate for small sample sizes when values of p are close to 0 or 1[83]. Note for sensitivity calculations, Animal 832 was considered positive because of it's MN-QuIC tonsil result (Table S4). GraphPad Prism version 9.0 for Windows (GraphPad Software, San Diego, California USA, www.graphpad.com) was used for conducting statistical analysis. Three technical replicates were used to demonstrate the potential application of AuNP on spontaneously misfolded rPrP. For initial trials on RPLN tissues from eight (four positive and four negative) animals, four and three technical replicates were used for RT-QuIC and AuNPs, respectively. For plate-based protocols, we tested palatine tonsils from ten positive and ten negative animals using four and eight replicates for RT-QuIC and AuNPs, respectively. We also tested 40 medial retropharyngeal lymph nodes (20 CWD positive and 20 CWD negative; Table S3) using four and eight replicates for RT-QuIC and AuNPs, respectively. Unless specified in figures, rate of amyloid formation and maximum wavelength of samples were compared to negative controls on their respective plate. The one-tailed Mann–Whitney unpaired u-test ($\alpha = 0.05$) was used to test the average difference for all parameters of interests between samples.

Field deployment. In March of 2021, we collaborated with the Minnesota DNR during annual CWD surveillance of the wild WTD population in Fillmore and Winona Counties, Minnesota. We assembled the necessary MN-QuIC equipment as described above on two portable tables within a DNR facility in Rushford, MN. RPLNs, parotid lymph nodes, and palatine tonsils were collected as described in Schwabenlander et al.[27], and were sampled and pooled together for each of the 13 animals tested. Tissues were homogenized in a BeadBug™ 3 Microtube homogenizer. All tissues were subject to 24 h MN-QuIC protocols as described above. Three replicates were performed for each of the 13 tissue pools and, for field-based analyses, a tissue pool was considered suspect CWD positive if one or more replicates was red. Tissues for suspected positive tissue pools were tested individually (Table S2). A tissue pool was considered CWD not-detected if all three replicates were blue or purple.

Animal research statement. No white-tailed deer were euthanized specifically for the research conducted herein and all tissues were secured from dead animals or loaned for our analyses. For these reasons, the research activities conducted herein are exempt from review by the University of Minnesota Institutional Animal Care and Use Committee (as specified https://research.umn.edu/units/iacuc/submit-maintain-protocols/overview). White-tailed deer were euthanized for annual culling efforts to control the spread of CWD in Minnesota following Minnesota Department of Natural Resources state regulations and euthanasia guidelines established by the Animal Care and Use Committee of the American Society of Mammalogists[84]. All methods and all experimental procedures carried out during the course of this research followed University of Minnesota guidelines and regulations as approved by the Institutional Biosafety Committee under protocol #1912-37662H. This study was also carried out in compliance with the ARRIVE guidelines (https://arriveguidelines.org).

Field research. White-tailed deer were euthanized by the state of Minnesota for routine annual culling efforts to control the spread of CWD and were not sampled specifically for the current study. Tissue samples were provided by the Minnesota Department of Natural Resources.

Data availability

All data generated or analyzed during this study are included in this published article and its supplementary information.

Received: 14 April 2022; Accepted: 8 July 2022
Published online: 18 July 2022

References

1. Prusiner, S. B. Nobel lecture: Prions. *Proc. Natl. Acad. Sci. USA* **95**, 13363–13383 (1998).
2. Telling, G. C. Breakthroughs in antemortem diagnosis of neurodegenerative diseases. *Proc. Natl. Acad. Sci. USA* **116**, 22894–22896 (2019).
3. Collinge, J. Prion diseases of humans and animals: Their causes and molecular basis. *Annu. Rev. Neurosci.* **24**, 519–550 (2001).
4. Williams, E. S. & Young, S. Chronic wasting disease of captive mule deer: A spongiform encephalopathy. *J. Wildl. Dis.* **16**, 89–98 (1980).
5. Fortin, J. S. *et al.* Equine pituitary pars intermedia dysfunction: A spontaneous model of synucleinopathy. *Sci. Rep.* **11**, 16036 (2021).
6. Haley, N. J. & Richt, J. A. Evolution of diagnostic tests for chronic wasting disease, a naturally occurring prion disease of cervids. *Pathogens* **6**, 35 (2017).

7. Haley, N. J. *et al.* Chronic wasting disease management in ranched elk using rectal biopsy testing. *Prion* **12**, 93–108 (2018).
8. Martinez, B. & Peplow, P. V. MicroRNAs in Parkinson's disease and emerging therapeutic targets. *Neural Regener. Res.* **12**, 1945–1959 (2017).
9. Hajipour, M. J. *et al.* Advances in Alzheimer's diagnosis and therapy: The implications of nanotechnology. *Trends Biotechnol.* **35**, 937–953 (2017).
10. Figgie, M. P. Jr. & Appleby, B. S. Clinical use of improved diagnostic testing for detection of prion disease. *Viruses* **13**, 789 (2021).
11. Parnetti, L. *et al.* CSF and blood biomarkers for Parkinson's disease. *Lancet Neurol.* **18**, 573–586 (2019).
12. Prusiner, S. B. *et al.* Scrapie prions aggregate to form amyloid-like birefringent rods. *Cell* **35**, 349–358 (1983).
13. Hannaoui, S., Schatzl, H. M. & Gilch, S. Chronic wasting disease: Emerging prions and their potential risk. *PLoS Pathog.* **13**, e1006619 (2017).
14. Joly, D. O. *et al.* Chronic wasting disease in free-ranging Wisconsin White-tailed Deer. *Emerg. Infect. Dis.* **9**, 599–601 (2003).
15. Osterholm, M. T. *et al.* Chronic wasting disease in cervids: Implications for prion transmission to humans and other animal species. *MBio* **10**, e01091-e1119 (2019).
16. Westergard, L., Christensen, H. M. & Harris, D. A. The cellular prion protein (PrPC): Its physiological function and role in disease. *Biochim. Biophys. Acta* **1772**, 629–644 (2007).
17. U.S. Fish and Wildlife Service & U.S. Census Bureau. *2016 National Survey of Fishing, Hunting and Wildlife-Associated Recreation*. https://www.census.gov/library/publications/2018/demo/fhw-16-nat.html (2018).
18. Wu, F. *et al.* Deer antler base as a traditional Chinese medicine: A review of its traditional uses, chemistry and pharmacology. *J. Ethnopharmacol.* **145**, 403–415 (2013).
19. Safar, J. G. *et al.* Prion clearance in bigenic mice. *J. Gen. Virol.* **86**, 2913–2923 (2005).
20. Haley, N. J. *et al.* Sensitivity of protein misfolding cyclic amplification versus immunohistochemistry in ante-mortem detection of chronic wasting disease. *J. Gen. Virol.* **93**, 1141–1150 (2012).
21. Saborio, G. P., Permanne, B. & Soto, C. Sensitive detection of pathological prion protein by cyclic amplification of protein misfolding. *Nature* **411**, 810–813 (2001).
22. Cheng, K. *et al.* Endpoint quaking-induced conversion: A sensitive, specific, and high-throughput method for antemortem diagnosis of Creutzfeldt-Jacob Disease. *J. Clin. Microbiol.* **54**, 1751–1754 (2016).
23. Vendramelli, R., Sloan, A., Simon, S. L. R., Godal, D. & Cheng, K. ThermoMixer-aided endpoint quaking-induced conversion (EP-QuIC) permits faster sporadic Creutzfeldt-Jakob disease (sCJD) identification than real-time quaking-induced conversion (RT-QuIC). *J. Clin. Microbiol.* **56**, e00423-e518 (2018).
24. Cheng, Y. C. *et al.* Early and non-invasive detection of chronic wasting disease prions in elk feces by real-time quaking induced conversion. *PLoS ONE* **11**, e0166187 (2016).
25. Atarashi, R. *et al.* Ultrasensitive human prion detection in cerebrospinal fluid by real-time quaking-induced conversion. *Nat. Med.* **17**, 175–178 (2011).
26. Li, M. *et al.* RT-QuIC detection of CWD prion seeding activity in white-tailed deer muscle tissues. *Sci. Rep.* **11**, 16759 (2021).
27. Schwabenlander, M. D. *et al.* Comparison of chronic wasting disease detection methods and procedures: Implications for free-ranging white-tailed deer (*Odocoileus virginianus*) surveillance and management. *J. Wildl. Dis.* **58**, 50–62 (2021).
28. Tsai, T.-T. *et al.* Diagnosis of tuberculosis using colorimetric gold nanoparticles on a paper-based analytical device. *ACS Sens.* **2**, 1345–1354 (2017).
29. Pelaz, B. *et al.* Diverse applications of nanomedicine. *ACS Nano* **11**, 2313–2381 (2017).
30. Howes, P. D., Chandrawati, R. & Stevens, M. M. Bionanotechnology. Colloidal nanoparticles as advanced biological sensors. *Science* **346**, 1247390 (2014).
31. Thiramanas, R. & Laocharoensuk, R. Competitive binding of polyethyleneimine-coated gold nanoparticles to enzymes and bacteria: A key mechanism for low-level colorimetric detection of gram-positive and gram-negative bacteria. *Microchim. Acta* **183**, 389–396 (2016).
32. Du, X.-J., Zhou, T.-J., Li, P. & Wang, S. A rapid Salmonella detection method involving thermophilic helicase-dependent amplification and a lateral flow assay. *Mol. Cell. Probes* **34**, 37–44 (2017).
33. Mayer, K. M. & Hafner, J. H. Localized surface plasmon resonance sensors. *Chem. Rev.* **111**, 3828–3857 (2011).
34. Myroshnychenko, V. *et al.* Modelling the optical response of gold nanoparticles. *Chem. Soc. Rev.* **37**, 1792–1805 (2008).
35. Lal, S., Link, S. & Halas, N. J. Nano-optics from sensing to waveguiding. *Nat. Photonics* **1**, 641–648 (2007).
36. Sepúlveda, B., Angelomé, P. C., Lechuga, L. M. & Liz-Marzán, L. M. LSPR-based nanobiosensors. *Nano Today* **4**, 244–251 (2009).
37. Dahlin, A. *et al.* Localized surface plasmon resonance sensing of lipid-membrane-mediated biorecognition events. *J. Am. Chem. Soc.* **127**, 5043–5048 (2005).
38. Zhao, W., Brook, M. A. & Li, Y. Design of gold nanoparticle-based colorimetric biosensing assays. *ChemBioChem* **9**, 2363–2371 (2008).
39. Zhang, H.-J. *et al.* Gold nanoparticles as a label-free probe for the detection of amyloidogenic protein. *Talanta* **89**, 401–406 (2012).
40. Flechsig, E. *et al.* Transmission of scrapie by steel-surface-bound prions. *Mol. Med.* **7**, 679–684 (2001).
41. Weissmann, C., Enari, M., Klöhn, P. C., Rossi, D. & Flechsig, E. Transmission of prions. *J. Infect. Dis.* **186**, S157–S165 (2002).
42. Luhr, K. M., Löw, P., Taraboulos, A., Bergman, T. & Kristensson, K. Prion adsorption to stainless steel is promoted by nickel and molybdenum. *J. Gen. Virol.* **90**, 2821–2828 (2009).
43. Masson, J.-F. Surface plasmon resonance clinical biosensors for medical diagnostics. *ACS Sens* **2**, 16–30 (2017).
44. Henderson, D. M. *et al.* Quantitative assessment of prion infectivity in tissues and body fluids by real-time quaking-induced conversion. *J. Gen. Virol.* **96**, 210–219 (2015).
45. Tennant, J. M. *et al.* Shedding and stability of CWD prion seeding activity in cervid feces. *PLoS ONE* **15**, e0227094 (2020).
46. Henderson, D. M. *et al.* Progression of chronic wasting disease in white-tailed deer analyzed by serial biopsy RT-QuIC and immunohistochemistry. *PLoS ONE* **15**, e0228327 (2020).
47. Wang, A., Perera, Y. R., Davidson, M. B. & Fitzkee, N. C. Electrostatic interactions and protein competition reveal a dynamic surface in gold nanoparticle-protein adsorption. *J. Phys. Chem. C* **120**, 24231–24239 (2016).
48. Abel, A. G. B. & Risselada, H. J. Gold-induced fibril growth: The mechanism of surface-facilitated amyloid aggregation. *Angew. Chem. Int. Ed.* **55**, 11242–11246 (2016).
49. Gasteiger, E. *et al.* Protein identification and analysis tools on the ExPASy server. In *The Proteomics Protocols Handbook* 571–607 (Humana Press, 2005).
50. Csapó, E. *et al.* Surface and structural properties of gold nanoparticles and their biofunctionalized derivatives in aqueous electrolytes solution. *J. Dispers. Sci. Technol.* **35**, 815–825 (2014).
51. Haley, N. J., Henderson, D. M., Senior, K., Miller, M. & Donner, R. Evaluation of Winter Ticks (*Dermacentor albipictus*) collected from North American Elk (Cervus canadensis) in an area of chronic wasting disease endemicity for evidence of PrPCWD amplification using real-time quaking-induced conversion assay. *mSphere* **6**, e0051521 (2021).
52. Rossi, M. *et al.* Ultrasensitive RT-QuIC assay with high sensitivity and specificity for Lewy body-associated synucleinopathies. *Acta Neuropathol.* **140**, 49–62 (2020).
53. Mok, T. H. *et al.* Bank vole prion protein extends the use of RT-QuIC assays to detect prions in a range of inherited prion diseases. *Sci. Rep.* **11**, 5231 (2021).

54. Haley, N. J., Mathiason, C. K., Zabel, M. D., Telling, G. C. & Hoover, E. A. Detection of sub-clinical CWD infection in conventional test-negative deer long after oral exposure to urine and feces from CWD+ deer. *PLoS ONE* **4**, e7990 (2009).
55. Spraker, T. R., Balachandran, A., Zhuang, D. & O'Rourke, K. I. Variable patterns of distribution of PrP(CWD) in the obex and cranial lymphoid tissues of Rocky Mountain elk (Cervus elaphus nelsoni) with subclinical chronic wasting disease. *Vet. Rec.* **155**, 295–302 (2004).
56. Sigurdson, C. J., Spraker, T. R., Miller, M. W., Oesch, B. & Hoover, E. A. PrPCWD in the myenteric plexus, vagosympathetic trunk and endocrine glands of deer with chronic wasting disease. *J. Gen. Virol* **82**, 2327–2334 (2001).
57. Picasso-Risso, C. *et al.* Assessment of real-time quaking-induced conversion (RT-QuIC) assay, immunohistochemistry and ELISA for detection of chronic wasting disease under field conditions in white-tailed deer: A Bayesian approach. *Pathogens* **11**, 489 (2022).
58. Chapinal, N., Schumaker, B. A., Joly, D. O., Elkin, B. T. & Stephen, C. Bayesian analysis to evaluate tests for the detection of *Mycobacterium bovis* infection in free-ranging wild bison (Bison bison athabascae) in the absence of a gold standard. *J. Wildl. Dis.* **51**, 619–625 (2015).
59. Branscum, A. J., Gardner, I. A. & Johnson, W. O. Estimation of diagnostic-test sensitivity and specificity through Bayesian modeling. *Prev. Vet. Med.* **68**, 145–163 (2005).
60. Joseph, L., Gyorkos, T. W. & Coupal, L. Bayesian estimation of disease prevalence and the parameters of diagnostic tests in the absence of a gold standard. *Am. J. Epidemiol.* **141**, 263–272 (1995).
61. Bloodgood, J., Kiupel, M., Melotti, J. & Straka, K. Chronic wasting disease diagnostic discrepancies: The importance of testing both medial retropharyngeal lymph nodes. *J. Wildl. Dis.* **57**, 194–198 (2021).
62. McNulty, E. *et al.* Comparison of conventional, amplification and bio-assay detection methods for a chronic wasting disease inoculum pool. *PLoS ONE* **14**, e0216621 (2019).
63. Zhang, X. Gold nanoparticles: Recent advances in the biomedical applications. *Cell Biochem. Biophys.* **72**, 771–775 (2015).
64. Li, J., Yan, X., Li, X., Zhang, X. & Chen, J. A new electrochemical immunosensor for sensitive detection of prion based on Prussian blue analogue. *Talanta* **179**, 726–733 (2018).
65. Zhao, J. *et al.* Graphene oxide-gold nanoparticle-aptamer complexed probe for detecting amyloid beta oligomer by ELISA-based immunoassay. *J. Immunol. Methods* **489**, 112942 (2021).
66. Ruppert, C., Phogat, N., Laufer, S., Kohl, M. & Deigner, H.-P. A smartphone readout system for gold nanoparticle-based lateral flow assays: Application to monitoring of digoxigenin. *Microchim. Acta* **186**, 119 (2019).
67. Mahato, K. *et al.* Gold nanoparticle surface engineering strategies and their applications in biomedicine and diagnostics. *3 Biotech* **9**, 57 (2019).
68. Adato, R. *et al.* Ultra-sensitive vibrational spectroscopy of protein monolayers with plasmonic nanoantenna arrays. *Proc. Natl. Acad. Sci. U. S. A.* **106**, 19227–19232 (2009).
69. Altug, H., Oh, S.-H., Maier, S. A. & Homola, J. Advances and applications of nanophotonic biosensors. *Nat. Nanotechnol.* **17**, 5–16 (2022).
70. Heo, C. *et al.* Identifying fibrillization state of Aβ protein via near-field THz conductance measurement. *ACS Nano* **14**, 6548–6558 (2020).
71. Wild, M. A., Spraker, T. R., Sigurdson, C. J., O'Rourke, K. I. & Miller, M. W. Preclinical diagnosis of chronic wasting disease in captive mule deer (*Odocoileus hemionus*) and white-tailed deer (*Odocoileus virginianus*) using tonsillar biopsy. *J. Gen. Virol.* **83**, 2629–2634 (2002).
72. Ferreira, N. C. *et al.* Detection of chronic wasting disease in mule and white-tailed deer by RT-QuIC analysis of outer ear. *Sci. Rep.* **11**, 7702 (2021).
73. Gao, D. *et al.* Studies on the interaction of colloidal gold and serum albumins by spectral methods. *Spectrochim. Acta A* **62**, 1203–1208 (2005).
74. Szekeres, G. P. & Kneipp, J. Different binding sites of serum albumins in the protein corona of gold nanoparticles. *Analyst* **143**, 6061–6068 (2018).
75. Kraus, A. *et al.* High-resolution structure and strain comparison of infectious mammalian prions. *Mol. Cell* **81**, 4540–4551 (2021).
76. Matthews, K. A. *et al.* Racial and ethnic estimates of Alzheimer's disease and related dementias in the United States (2015–2060) in adults aged ≥65 years. *Alzheimers. Dement.* **15**, 17–24 (2019).
77. Orrú, C. D. *et al.* Human variant Creutzfeldt-Jakob disease and sheep scrapie PrP(res) detection using seeded conversion of recombinant prion protein. *Protein Eng. Des. Sel.* **22**, 515–521 (2009).
78. Hwang, S., Greenlee, J. J. & Nicholson, E. M. Use of bovine recombinant prion protein and real-time quaking-induced conversion to detect cattle transmissible mink encephalopathy prions and discriminate classical and atypical L- and H-Type bovine spongiform encephalopathy. *PLoS ONE* **12**, e0172391 (2017).
79. Kraus, A. *et al.* Seeding selectivity and ultrasensitive detection of tau aggregate conformers of Alzheimer disease. *Acta Neuropathol.* **137**, 585–598 (2019).
80. Fairfoul, G. *et al.* Alpha-synuclein RT-QuIC in the CSF of patients with alpha-synucleinopathies. *Ann. Clin. Transl. Neurol.* **3**, 812–818 (2016).
81. Špringer, T. & Homola, J. Biofunctionalized gold nanoparticles for SPR-biosensor-based detection of CEA in blood plasma. *Anal. Bioanal. Chem.* **404**, 2869–2875 (2012).
82. Sergeant. *Epitools Epidemiological Calculators*. epitools.ausvet.com.http://epitools.ausvet.com.au (2018).
83. Brown, L. D., Tony Cai, T. & DasGupta, A. Interval estimation for a binomial proportion. *Stat. Sci.* **16**, 101–133 (2001).
84. Sikes, R. S. & Animal Care and Use Committee of the American Society of Mammalogists. 2016 Guidelines of the American Society of Mammalogists for the use of wild mammals in research and education. *J. Mammal.* **97**, 663–688 (2016).

Acknowledgements

Funding for research performed herein was provided by the Interdisciplinary Doctoral Fellowship from the University of Minnesota to P.R.C., the Minnesota State Legislature through the Minnesota Legislative-Citizen Commission on Minnesota Resources (LCCMR), Minnesota Agricultural Experiment Station Rapid Agricultural Response Fund, the Sanford P. Bordeau Chair in Electrical Engineering at the University of Minnesota to S.-H.O., and start-up funds awarded to P.A.L. through the Minnesota Agricultural, Research, Education, Extension and Technology Transfer (AGREETT) program. We thank C. Ertsgaard and D. J. Lee for helpful discussions on experimental results and protocols. Portions of this work were conducted in the Minnesota Nano Center, which is supported by the National Science Foundation through the National Nano Coordinated Infrastructure Network (NNCI) under Award Number ECCS-2025124. W. Zhang provided the expertise for TEM studies. Portions of this work were carried out in the University of Minnesota Characterization Facility, which receives partial support from the NSF through the MRSEC (Award Number DMR-2011401) and the NNCI (Award Number ECCS-2025124) programs. F. Schendel, T. Douville, and staff of the University of Minnesota Biotechnology Resource Center provided critical support concerning the large-scale production of recombinant proteins. We thank the Minnesota Department of Natural Resources, especially M. Carstensen, L. Cornicelli, E. Hildebrand, P.

Hagen, and K. LaSharr, for providing the white-tailed deer tissues used for our analyses and logistical assistance for MN-QuIC field deployment. K. Wilson of the Colorado State University Veterinary Diagnostic Laboratory provided assistance with ELISA and IHC testing of samples reported herein. S. Stone provided valuable logistical assistance with our molecular work. We thank NIH Rocky Mountain Labs, especially B. Caughey, A. Hughson, and C. Orru for training and assistance with the implementation of RT-QuIC and for supplying the original rPrP clone. Figure 1 and parts of Fig. 2 were created using BioRender (BioRender.com).

Author contributions

P.R.C. and M.L. conceived the study. P.R.C., M.L., and G.R. performed molecular experiments. P.R.C., M.L., M.S., S.H.O., and P.A.L. assisted with experimental design and interpreted the results. P.R.C., M.L., M.S., T.M.W., and P.A.L. conducted field-based testing of the diagnostics presented herein. P.R.C. and M.L. performed statistical analyses. S.H.O. and P.A.L. oversaw the research. All authors wrote and contributed to the final manuscript.

Competing interests

The authors declare no competing interests.

Additional information

Supplementary Information The online version contains supplementary material available at https://doi.org/10.1038/s41598-022-16323-y.

Correspondence and requests for materials should be addressed to S.-H.O. or P.A.L.

Reprints and permissions information is available at www.nature.com/reprints.

Publisher's note Springer Nature remains neutral with regard to jurisdictional claims in published maps and institutional affiliations.